The Planetary Science Journal, 2:152 (30pp), 2021 August https://doi.org/10.3847/PSJ/ac0ea0

Ultra-short-period Planets in K2. III. Neighbors are Common with 13 New Multiplanet Systems and 10 Newly Validated Planets in Campaigns 0–8 and 10

Elisabeth R. Adams[1], Brian Jackson[2], Samantha Johnson[3,4], David R. Ciardi[5], William D. Cochran[6], Michael Endl[7], Mark E. Everett[8], Elise Furlan[9], Steve B. Howell[10], Prasanna Jayanthi[2], Phillip J. MacQueen[7], Rachel A. Matson[11], Ciera Partyka-Worley[2], Joshua Schlieder[12], Nicholas J. Scott[10], Sevio M. Stanton[2], and Carl Ziegler[13]
[1] Planetary Science Institute, 1700 E. Ft. Lowell, Suite 106, Tucson, AZ 85719, USA; adams@psi.edu
[2] Department of Physics, Boise State University, 1910 University Drive, Boise ID 83725, USA
[3] Department of Physics, University of North Carolina at Chapel Hill, Chapel Hill, North Carolina 27599, USA
[4] Triangle Universities Nuclear Laboratory, Duke University, Durham, North Carolina 27708, USA
[5] NASA Exoplanet Science Institute, 770 South Wilson Avenue, Pasadena, CA 91125, USA
[6] Center for Planetary Systems Habitability and McDonald Observatory, The University of Texas at Austin, Austin, TX 78712, USA
[7] McDonald Observatory, The University of Texas at Austin, Austin, TX 78712, USA
[8] NSF's Optical Infrared Astronomy Research Laboratory, 950 North Cherry Avenue, Tucson, AZ 85719, USA
[9] NASA Exoplanet Science Institute, Caltech/IPAC, 770 South Wilson Avenue, Pasadena, CA 91125, USA
[10] NASA Ames Research Center, Moffett Field, CA 94035, USA
[11] U.S. Naval Observatory, 3450 Massachusetts Avenue NW, Washington, DC 20392, USA
[12] NASA Goddard Space Flight Center, Greenbelt, MD, USA
[13] Dunlap Institute for Astronomy and Astrophysics, University of Toronto, 50 St. George Street, Toronto, Ontario M5S 3H4, Canada
Received 2020 November 19; revised 2021 May 14; accepted 2021 May 19; published 2021 August 6

Abstract

Using the EVEREST photometry pipeline, we have identified 74 candidate ultra-short-period planets (USPs; orbital period $P < 1$ day) in the first half of the K2 data (Campaigns 0–8 and 10). Of these, 33 candidates have not previously been reported. A systematic search for additional transiting planets found 13 new multiplanet systems containing a USP, doubling the number known and representing a third (32%) of USPs in our sample from K2. We also identified 30 companions, which have periods from 1.4 to 31 days (median 5.5 days). A third (36 of 104) of the candidate USPs and companions have been statistically validated or confirmed in this work, 10 for the first time, including 7 USPs. Almost all candidates, and all validated planets, are small (radii $R_p \leqslant 3\,R_\oplus$) with a median radius of $R_p = 1.1\,R_\oplus$; the validated and confirmed USP candidates have radii between $0.4\,R_\oplus$ and $2.4\,R_\oplus$ and periods from $P = 0.18$ to 0.96 days. The lack of candidate (a) ultra-hot-Jupiter ($R_p > 10\,R_\oplus$) and (b) short-period-desert ($3 \leqslant R_p \leqslant 10\,R_\oplus$) planets suggests that both populations are rare, although our survey may have missed some of the very deepest transits. These results also provide strong evidence that we have not reached a lower limit on the distribution of planetary radius values for planets at close proximity to a star and suggest that additional improvements in photometry techniques would yield yet more USPs. The large fraction of USPs in known multiplanet systems supports origins models that involve dynamical interactions with exterior planets coupled to tidal decay of the USP orbits.

Unified Astronomy Thesaurus concepts: Transit photometry (1709); Exoplanet catalogs (488); Exoplanet formation (492); Exoplanet evolution (491)

Supporting material: machine-readable tables

1. Background

With about 200 planets known with orbital periods less than a day (Figure 1), it seems that planets can occupy every available nook and cranny of their stellar systems. These ultra-short-period planets (USPs) lie at the edge of orbital stability and have defied easy explanation, although it seems unlikely that they formed where we find them (Jackson et al. 2016). Empirically, USPs around main-sequence stars can be divided into three populations by size. (1) Small USPs (⩽2–3 Earth radii, or $R_\oplus$) have been found with stable orbits down to orbital period $P = 4.2$ hr or 0.17 days (KOI 1843.03, Rappaport et al. 2013). (2) Large USPs, or ultra-hot Jupiters (UHJs; $R_p \geqslant 10\,R_\oplus$) have been confirmed with periods as short as $P = 19$ hr or 0.767 days (NGTS-10 b, McCormac et al. 2020), near where Roche lobe overflow may begin (Rappaport et al. 2013). (3) Very few intermediate-sized planets ($R_p =$ 3–10 $R_\oplus$) have been confirmed, a gap known as the short-period or sub-Jovian desert that extends out to $P = 2$–3 days (e.g., Lopez & Fortney 2014; Mazeh et al. 2016). Although the physical mechanisms that shape the desert are still uncertain, the location of the gap corresponds to the radius values expected for planets that are too large to be predominantly rocky. Just three confirmed planets are known in the inner desert ($P < 1.5$ days): LTT 9779b ($R_p = 4.59 \pm 0.23\ R_\oplus$, $M_p = 29.32^{+0.78}_{-0.81} M_\oplus$, $P = 0.79$ days; Jenkins 2019), TOI-849 b ($R_p = 3.44^{+0.157}_{-0.115}\ R_\oplus$, $M_p = 40.8^{+2.4}_{-2.5} M_\oplus$, $P = 0.7655$ days; Armstrong et al. 2020), and K2-266 b from the K2 Campaign 14 ($R_p = 3.3 \pm 1.8\ R_\oplus$, $P = 0.658$ days; Rodriguez et al. 2018).

Of the three leading classes of theory to explain the existence of USPs—in situ formation, migration powered by tides raised on the host stars, or tidal migration coupled with multibody interactions—the first is unlikely due to the extreme temperatures at such short orbital periods (Boss 1998) and likely

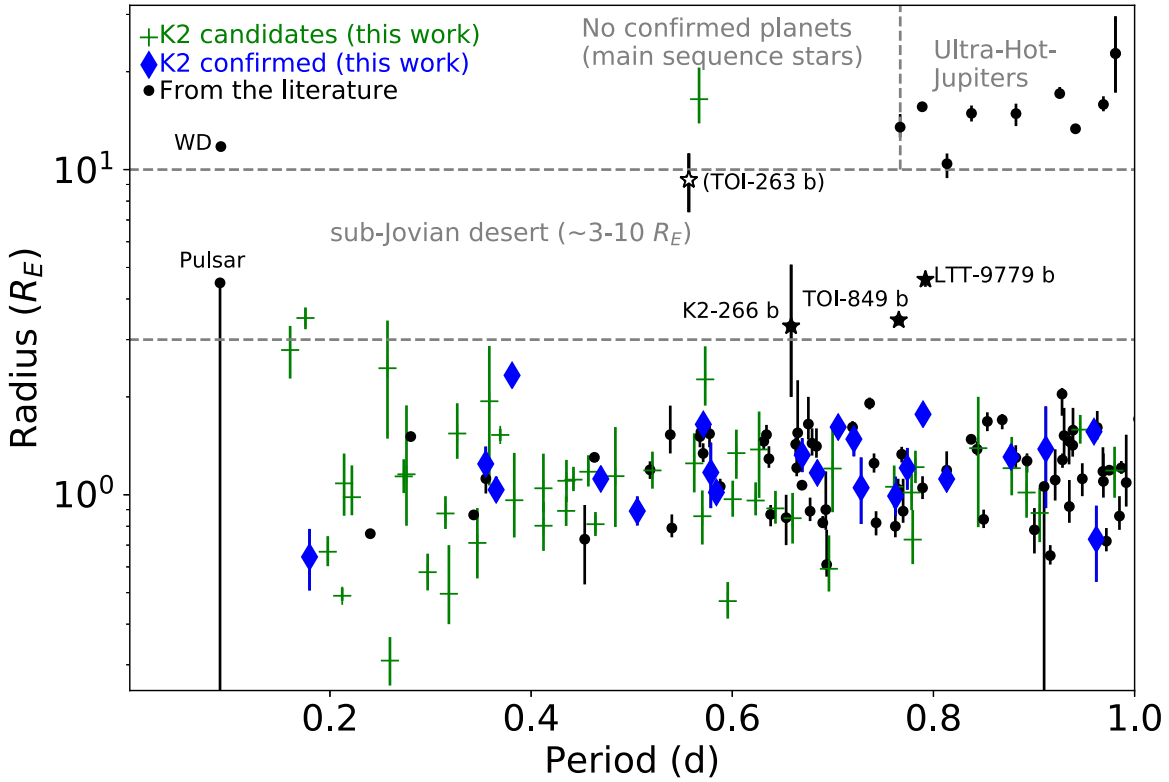

Figure 1. USPs ($P > 1$ day). All confirmed (blue diamond) and candidate (green plus sign) USPs from this work for K2 C0–8 and 10 are shown, along with confirmed planets from the literature (black circles). The few known candidate (open black star) and confirmed (closed black star) planets in the sub-Jovian desert (roughly $3 < R_p < 10\,R_\oplus$ and $P < 1.6$ days) are also shown. The only confirmed planets with $P < 0.15$ days are around pulsars or white dwarfs. Data compiled from exoplanetarchive.ipac.caltech.edu/, exoplanet.eu, and this work.

truncation of the protoplanetary disk much farther out (Lee & Chiang 2017). However, the roles of tidal migration in the planets' origins are the subjects of active research (e.g., Dawson & Johnson 2018). Whatever its origins, once a planet occupies a short-period orbit, the host star's influence may remove it in a few billion years, with two chief mechanisms theorized. For volatile-rich planets, high atmospheric temperatures and intense stellar irradiation can lead to atmospheric loss (Owen 2019). Strong tidal forces lead to orbital decay, driving the planet into unstable Roche lobe overflow, with complete disruption of the atmosphere occurring in just a few orbits (Jia & Spruit 2017).

The long-term stability of USPs is highly uncertain (Adams & Bloch 2015). Hamer & Schlaufman (2019) determined that the population of hot-Jupiter host stars is younger than either the population all field stars or the population of all stars known to host planets. This result suggests that close, giant planets quickly inspiral or are otherwise destroyed, while their stars are still on the main sequence. Moreover, at least two main-sequence stars have small USPs that appear to be actively disintegrating, as seen by distinctive features in their transit light curves (Rappaport et al. 2012; Sanchis-Ojeda et al. 2015a). The environment in which USPs find themselves is clearly perilous, but at the same time, hundreds of USPs—which may orbit 0.1%–1% of all Sun-like stars (Sanchis-Ojeda et al. 2014)—have been found and require explanation.

Studying USPs, both individually and as a population, thus presents unique opportunities to observe the end state of planet evolution. Of particular use for testing theoretical models are the relative abundance of USPs of different masses and orbital periods, and the architecture (sizes, separations, and mutual inclinations) of multiplanet systems that contain a USP. Systems hosting USPs are also ideal for radial-velocity (RV) follow-up (assuming the star is bright enough) to determine masses, long-term timing measurements to watch for orbital decay (e.g., WASP-12 b; Patra et al. 2017; Baluev et al. 2019), and ultimately direct measurements of atmospheric escape using JWST or other next-generation telescopes.

Fortunately, USPs are a particularly advantageous group to observe. Their short orbital periods make it easy to observe multiple planetary orbits, allowing for a more rapid determination of precise planetary parameters. Even very small USPs are relatively easy to detect in space-based data sets such as those provided by Kepler, K2, and TESS, which span several months to several years of continuous observations and therefore contain hundreds to thousands of individual transits. Some USPs have transit depths of less than 100 parts per million (ppm), and the typical depth is only a few hundred ppm, which means that stacking multiple transits together is often required for transit light-curve fits. USPs also have larger RV signatures than more distant planets of the same size, facilitating mass estimation. Kepler-78 b is one of the smallest exoplanets with a measured mass, about 1.7 $M_\oplus$ (Howard et al. 2013; Pepe et al. 2013), and the planet's extremely short period, 8.5 hr, allowed its RV signal to be disentangled from the star's longer-term activity cycle. Other measurements of planetary properties are easier at ultra-short periods: an 8 M_E (Endl et al. 2012) member of a five-planet system, 55 Cnc e, has $P = 17$ hr and such a high brightness temperature (~1800 K) that its eclipse (the occultation of the planet by the star) was detected in IR by the Spitzer Space Telescope (Demory et al. 2016a), the smallest planet for which that has been possible. Demory et al. (2016b)

reported that the planet's eclipse exhibits year-to-year IR variability, a result recently corroborated by Tamburo et al. (2018) and potentially signaling active volcanism. Given their observational prominence, it is important to understand whether small USPs are representative of all small exoplanets or whether they constitute a unique species. They are critical tracers of theories of planet formation and evolution.

In this study, we continue the work of the Short-Period Planet Group (SuPerPiG) collaboration (Jackson et al. 2013; Adams et al. 2016, 2017) to discover, corroborate, and characterize USPs using data from the K2 Mission. We analyzed observations from Campaigns 0–8 and 10 of K2 (ignoring the microlensing campaign in C9) using the improved EVEREST 2.0 pipeline (Luger et al. 2016, 2018) and compared the results to different analyses using the k2sff pipeline (Vanderburg & Johnson 2014) and the EVEREST 1.0 pipeline (Kruse et al. 2019). In this work, using the EVEREST 2.0 photometry has resulted in twice as many USPs smaller than Earth as Mayo et al. (2018) (see Section 6.5), and roughly six times as many sub-Earths and twice as many 1–2 $R_\oplus$ planets as our previous USP survey (Adams et al. 2016) (see Section 7), which both used k2sff photometry. To estimate the false-positive probability (FPP) for each candidate, we use statistical validation by employing the vespa model (Morton 2012). We find that, of 74 total USP candidates, 21 have FPPs <1%, suggesting they are bona fide planets. An additional 15 out of 30 companion planets in the same systems were also validated. (Note: although many works use the 1% validation threshold, including Montet et al. 2015; Hirano et al. 2018; Livingston et al. 2018, a few use a more stringent 0.1% cutoff, e.g., Mayo et al. 2018; if we were to use the same threshold, only 22 of 104 candidates would have been validated by this work and that would not include 12 planets that have been reported confirmed or validated in other works.) At the other extreme, 17 candidates have FPP >50% and 5 have FPP >90%, suggesting that they are unlikely to be planets. The faintest object we validated has Kepler magnitude Kep = 17.3, and most of the host stars for our candidate planets are sufficiently bright for ground-based imaging to provide effective imaging constraints, while about half have magnitudes suitable for ground-based spectroscopy (Kep < 14).

The plan for this paper is as follows: in Section 2, we detail our transit search procedure. Our systematic search for additional transiting companions is described in Section 3. In Section 4, we present our ground-based follow-up observations. In Section 5, we discuss our statistical validation results. We discuss individual candidates in Section 6. In Section 7, we estimate our survey's completeness. Finally, in Section 8, we explore the properties of the K2 population of USPs as a whole and examine the implications for planet formation theories, with a focus on the USP systems hosting multiple planets.

2. Photometry and Transit Search

The candidate search method used in this paper is similar to prior SuPerPiG papers (Adams et al. 2016, 2017), with one key difference: the choice of photometry pipeline. As a test of the precision of the EVEREST pipeline, we searched both k2sff and EVEREST 2.0 photometry, using data from Campaigns C0–8 and 10. EVEREST 2.0 claims 10%–20% better photometric precision than EVEREST 1.0, which in turn claimed to be 25% better than k2sff—and for the mostly small USP population, these differences are highly significant in terms of the number of planets detected.

The discovery method employed is as follows: we retrieved the EVEREST 2.0 (hereafter referred to as EVEREST) photometry (Luger et al. 2016, 2018) from MAST[14] and the k2sff photometry (Vanderburg & Johnson 2014) from MAST[15] for Campaigns 0–8 and 10. For each of the 10,000–30,000 light curves per campaign, we subtracted a median boxcar filter with a window size of 1 day. A window size of a day is well-suited to USPs and other short-period planets, with transit durations of 1–3 hr. It might not be appropriate for long-period planets where the transit duration could be an appreciable fraction of a day and could result in lower yields, particularly of shallow transits. The performance of our pipeline at periods beyond a few days is left for future research.

We estimated the overall scatter, σ, using 1.4826 times the median absolute deviation and masked out individual points that lay $\geqslant 10\sigma$ from the campaign median value. The choice to cut points more than 10σ out of transit was made to facilitate small-planet discovery and had the desired side effect of eliminating many eclipsing binary blends before the vetting process, the inclusion of which would have increased the workload on the survey by a factor of several. However, we may also have inadvertently eliminated some of the deepest UHJ candidates. Many deep transits were nonetheless identified as periodic candidates, as a substantial fraction of the points in transit during ingress and egress are within 10σ of the baseline, which causes the light curve to show up with the bottom removed. In such cases, we reanalyzed the light curve with a much higher noise clipping (50σ) so that we could fit the transit (e.g., the 4.5 day companion EPIC 206103150/HD 3167 b). Almost all those candidates were then subsequently eliminated upon finding clear signs of phase variability or odd/even transit depth differences that are associated with eclipsing binaries. The largest viable candidate in this work has a depth of 6400 ppm (EPIC 210605073).

We next searched for transit signals with orbital periods between 3 and 72 hr using the EEBLS algorithm (Kovács et al. 2002). Although the goal of this work is to discover planets with $P \leqslant 24$ hr, we first examined candidates at longer periods to identify potential aliased signals, which are particularly common at twice the true orbital period. Issues with aliasing USPs to longer periods have been a problem since the identification of the very first USP, 55 Cnc e (Dawson & Fabrycky 2010).

To maximize the yield of USPs, which are intrinsically uncommon (e.g., Sanchis-Ojeda et al. 2014), and because many candidates are easily recovered at a lower signal-to-noise threshold, we relaxed the discovery threshold to $\geqslant 7\sigma$, as opposed to $\geqslant 10\sigma$ in, e.g., Adams et al. (2017). We found 104 candidates with transit-like signals and $P < 1$ day that met that transit depth threshold in at least one pipeline and subjected each one to further vetting by hand by some of the co-authors of this paper, with each candidate examined by at least two people. During this vetting step, transits were binned at low multiples of the nominal orbital period to search for masquerading binary stars, and the transit depth, duration, and odd–even differences were also examined for discrepancies.

For the surviving candidates, we fit the transit light curve using Markov Chain Monte Carlo (MCMC) methods. In the first iteration of this search using the k2sff pipeline, we used the

[14] http://archive.stsci.edu/k2/hlsp/everest/search.php
[15] http://archive.stsci.edu/k2/hlsp/k2sff/search.php

algorithm from Mandel & Agol (2002) as implemented by the Python packages Batman (Kreidberg 2015) and PyLightCurve (https://github.com/ucl-exoplanets/pylightcurve); in those fits, which are retained in this publication only for comparison to the EVEREST results, we used 100,000 links in each chain, thinning the sample by a factor of 10 and then discarding as burn-in the first 1000 iterations. For the bulk of our analysis using EVEREST, we fit the light curves using the PyLightcurve package, which is based on Emcee, an affine-invariant ensemble sampler (Foreman-Mackey et al. 2013). We used 600,000 iterations and 1500 walkers and discarded the first half (300,000 iterations) as burn-in. (No significant difference was seen in the fit results between the two methods; the switch was made for reasons of software compatibility and run-time improvements.)

We fixed the eccentricity for all fits at zero, because the orbits for all USPs are expected to be tidally circularized (Jackson et al. 2008); whether any of the more distant companions may have nonzero eccentricity is left for future work. The limb-darkening coefficients were calculated using the stellar parameters in Table 1 using coefficients from Claret & Bloemen (2011). During fitting, the inclination was allowed to range freely above 90°, as transit photometry cannot distinguish between prograde and retrograde orbits. For a few companions with low signal-to-noise ratios (S/Ns), the quality of the light curve was poor enough that we fixed the inclination (to $i = 90°$) and a/R_* (to a reasonable guess scaled from the periods of both planets and a/R_* values of the USP) and fit only for R_P/R_* and $T_{\rm mid}$; those fits are noted in Table 2. The best-fit model parameters in Table 2 are calculated using a confidence interval of 68% of the posterior values, where the value reported is at 50% of the distribution. For parameters that are derived from the fitted parameters, namely the radius in $R_\oplus$ (which depends on $R_\odot$) and the transit duration (which depends on a/R_*, i, and R_p/R_*), the errors are calculated by sampling from the appropriate chains for the dependent variables. For the planet radius, two half-Gaussian distributions were constructed around the asymmetric error on the stellar radius; we generated 150,000 points for both half distributions and randomly assigned one point to each link in the radius ratio chain. For the transit duration, a random value from each of the inclination, semimajor axis, and radius ratio chains was drawn to create a duration chain of equal length, using the fixed value for the few cases where those values were not fitted.

To check convergence, we use the autocorrelation statistic test in Emcee, checking that the correlation length is always much less than the length of the chain, and found values between 1 and 15, indicating that the 300,000-link chains were likely well converged. We also visually inspected the traces for each parameter and the correlations between parameters (the so-called triangle plot).

We examined additional information on each system, including the EVEREST data validation (DV) reports (which include photometry and images of the aperture) and stellar observations that had either been reported to the ExoFOP[16] or were made for the purpose of this work (see Section 4.1). If more than one transiting candidate was detected in the system, we reported fits for each planet candidate (see Section 3).

Although our final results are based on the EVEREST light curves, we found it useful to compare those results to the fits to the k2sff curves because they were derived from an independent pipeline with different aperture sizes and calibration choices; background blends are likely to be blended by different amounts, while the parameters for true planets should remain constant. Out of 93 signals originally flagged for follow-up, 35 were only detected in EVEREST, while 5 were only detected in k2sff. For the majority of signals which were detected in both pipelines, we compared the planetary properties and flagged any significant discrepancies. For example, if the fitted depths disagreed by more than 50%, that was considered a clear sign of an eclipsing binary that has a different blended fraction in each pipeline. When the period differed by more than a few minutes, it was typically a sign of a spurious detection picking up on noise or other nontransiting features. Of the five signals detected only in the k2sff pipeline, all were clearly tagged as false positives during the initial vetting due to features in the folded EVEREST light curves; among them was EPIC 211995325, previously reported as a planet using k2sff data by Adams et al. (2016). Meanwhile, most of the EVEREST-only signals (30 of 35) remained viable candidates after vetting and are therefore more likely to be real planets that were just below the k2sff detectability threshold. We conclude that the EVEREST photometry is preferable for small-planet searches, and we use it in all analyses and results presented in this paper going forward, with one exception noted in Section 6.4.3. (However, we note that eight of the EVEREST-only candidates have high FPPs, as discussed in Section 6.4.4.)

3. Systematic Search for Additional Transiting Planets

3.1. The Importance of Multiplanet Systems

Multiplanet systems are important for several reasons. First, the system architecture (orbits, sizes, and compositions) is key to unlocking the formation history of these systems. Second, the mere presence of one or more additional planets boosts the likelihood that all candidates are planets (Lissauer et al. 2012) We follow the revised analysis of Burke et al. (2019) and assign likelihood boost factors of 10 for two-candidate systems and 15 for three or more candidates. We do not apply a validation boost, however, for candidates detected with S/N $\leqslant$ 10; see Section 5 for a discussion of the effect of low S/N on validation of both single and multiplanet systems. In Table 2, we report the individual and boosted FPP, where applicable, for each candidate.

3.1.1. Identification of Potential Multiplanet Systems Has Often Been Piecemeal

Previous work has turned up numerous cases of USPs in multiplanet systems, often identified because the companion planet (s) had obvious transits in the photometry (e.g., Adams et al. 2017). It is also common, however, for multiple candidates at different periods to be reported individually in separate works, with no combined system analysis performed or even consistent candidate numbering (e.g., EPIC 206215704/K2-302; see Section 6.3.3). Motivated by these discrepancies, for the first time we have systematically searched every candidate USP in K2 Campaigns 0–8 and 10 for evidence of transiting companions.

We note that for completeness, a full census of USPs in multiplanet systems would require searching all known transiting planet candidates at any period for heretofore missed USPs, using the targeted short-period search methods described

[16] https://exofop.ipac.caltech.edu/

Table 1
Candidate Host Star Parameters

Candidate	C.	R.A.	Decl.	$m_{\rm Kep}$	$R_\star$ ($R_\odot$)	$T_{\rm eff}$	[Fe/H]	log(g)	u_1[a]	u_2	u_3	u_4	Name	Source[b]
201085153	C10	180.122852	−7.012986	17.33	0.38 ± 0.15	3945 ± 386	-0.2 ± 0.35	4.9 ± 0.2	0.66	0.394	−0.364	0.137		E
201089381	C10	181.393564	−6.894076	14.28	0.77 ± 0.14	5709 ± 170	-0.8 ± 0.42	4.5 ± 0.1	0.202	1.06	−0.798	0.224		E
201110617	C10	182.700187	−6.294205	12.95	0.62 ± 0.02	4460 ± 50	-0.33 ± 0.08	4.7 ± 0.1	0.62	−0.489	1.13	−0.435	K2-156	M18
201130233	C10	183.751337	−5.781991	12.6	0.88 ± 0.04	5456 ± 50	0.13 ± 0.08	4.5 ± 0.1	0.612	−0.325	0.944	−0.446	K2-157	M18
201214691	C1	174.871463	−3.755974	14.23	0.78 ± 0.05	5122 ± 82	-0.049 ± 0.25	4.5 ± 0.04	0.612	−0.453	1.16	−0.519		E,B
201230694	C1	171.09001	−3.501374	15.18	0.48 ± 0.04	4086 ± 80	-0.1 ± 0.18	4.8 ± 0.05	0.614	0.18	0.033	0.004		E
201231940	C1	174.120612	−3.482449	18.11	0.27 ± 0.02	3927 ± 39	-0.56 ± 0.05	5 ± 0.1	0.881	0.123	−0.324	0.147		E
201239401	C1	173.052956	−3.370242	15.04	0.33 ± 0.06	3782 ± 90	-0.13 ± 0.2	5 ± 0.02	0.551	0.731	−0.694	0.226		E
201264302	C1	169.598013	−2.991577	13.88	0.188 ± 0.004	3875 ± 157	-0.8 ± 0.2	4.2 ± 0.2	0.791	0.147	−0.226	0.127		M
201427007	C10	184.602205	−0.551349	14.22	0.94 ± 0.09	5633 ± 111	-0.053 ± 0.24	4.4 ± 0.07	0.517	0.007	0.532	−0.299		E
201438507	C10	182.714439	−0.383279	14.07	0.89 ± 0.1	5532 ± 113	-0.13 ± 0.32	4.5 ± 0.07	0.514	−0.024	0.597	−0.328		E
201461352	C1	175.686546	−0.0553	17.15	0.155 ± 0.003	3092 ± 37	-0.036 ± 0.14	5.2 ± 0.02	0.432	0.793	−0.518	0.108		E
201469738	C1	177.738562	0.068657	15.82	0.48 ± 0.05	4050 ± 166	-0.011 ± 0.2	4.8 ± 0.04	0.587	0.21	0.041	−0.008		E
201549425	C1	176.938421	1.278706	15.47	0.5 ± 0.08	4415 ± 178	-0.55 ± 0.3	4.8 ± 0.1	0.591	−0.203	0.693	−0.27		E
201595106	C10	183.720347	1.96828	11.68	0.93 ± 0.06	5820 ± 20	-0.01 ± 0.03	4.6 ± 0.1	0.493	0.135	0.341	−0.226		M,M18
201609593	C1	173.066309	2.192621	14.71	0.29 ± 0.01	3630 ± 36	0.007 ± 0.05	5 ± 0.04	0.465	0.758	−0.542	0.131		E
201637175	C1	169.482818	2.61907	14.93	0.58 ± 0.03	3879 ± 90	0.032 ± 0.12	4.7 ± 0.04	0.553	0.285	0.021	−0.030	K2-22A	Dr17
201650711	C1	172.044052	2.826891	12.25	0.34 ± 0.05	4310 ± 92	-0.82 ± 0.05	4.2 ± 0.3	0.581	−0.272	0.826	−0.323		M
201687804	C1	175.012744	3.434154	13.13	0.63 ± 0.06	4483 ± 184	-0.01 ± 0.09	4.7 ± 0.04	0.674	−0.682	1.34	−0.491		E
201717159	C1	178.436482	3.932202	15.98	0.46 ± 0.07	4092 ± 198	-0.15 ± 0.2	4.8 ± 0.06	0.635	0.164	0.021	0.0108		E
201796374	C1	171.527163	5.301112	16.37	0.26 ± 0.02	3587 ± 71	-0.057 ± 0.08	5 ± 0.02	0.46	0.793	−0.588	0.148		E
201923289	C1	174.920526	7.825885	13.69	0.85 ± 0.07	5350 ± 127	-0.021 ± 0.15	4.5 ± 0.03	0.591	−0.315	0.968	−0.46		E
203533312	C2	243.955378	−25.818471	12.16	1.3 ± 0.1	6620 ± 86	0.09 ± 0.05	4.2 ± 0.1	0.412	0.691	−0.591	0.186		M,I20
205002291	C2	247.749587	−19.875631	14.27	0.31 ± 0.06	3685 ± 108	-0.002 ± 0.1	5 ± 0.04	0.482	0.744	−0.559	0.145		E
205152172	C2	245.180008	−19.14414	13.49	0.53 ± 0.09	4202 ± 242	-0.04 ± 0.2	4.8 ± 0.04	0.613	−0.11	0.485	−0.149		E
206024342	C3	331.277219	−14.121665	13.05	1.1 ± 0.36	5724 ± 72	-0.22 ± 0.06	4.5 ± 0.1	0.431	0.291	0.181	−0.168	K2-299	M
206042996	C3	337.513575	−13.610113	16.06	0.5 ± 0.04	4114 ± 99	0.006 ± 0.12	4.8 ± 0.05	0.592	0.059	0.264	−0.081	K2-301	E
206103150	C3	331.203044	−12.018893	11.76	1.1 ± 0.04	5565 ± 60	0.43 ± 0.04	4.3 ± 0.07	0.68	−0.457	1.06	−0.479	WASP-47	S15,M13
206151047	C3	333.71501	−10.769168	13.43	1.2 ± 0.55	5971 ± 67	-0.25 ± 0.06	4.6 ± 0.09	0.367	0.576	−0.24	0.006		M
206215704	C3	335.094822	−9.509531	15.6	0.25 ± 0.01	3297 ± 73	-0.33 ± 0.093	4.9 ± 0.08	0.487	0.846	−0.718	0.203	K2-302	D19
206298289	C3	337.357688	−8.266702	14.69	0.33 ± 0.03	3875 ± 157	-1 ± 0.1	4.4 ± 0.2	0.92	0.098	−0.369	0.189		M
206417197	C3	337.133466	−6.347505	13.35	0.75 ± 0.04	5245 ± 55	-0.15 ± 0.05	4.6 ± 0.07	0.566	−0.29	0.975	−0.468		M
210605073	C4	65.62329	17.037875	17.89	$1.6^{+0.42}_{-0.24}$	7918 ± 500	0 ± 0	0 ± 0	0.417	0.766	−0.825	0.291		Inf.,I
210707130	C4	59.464394	18.465254	12.1	0.68 ± 0.03	4427 ± 48	-0.36 ± 0.05	4.3 ± 0.1	0.646	−0.658	1.37	−0.525	K2-85	M,Dr17
210801536	C4	52.818936	19.891303	13.18	$0.85^{+0.28}_{-0.09}$	5304 ± 259	-0.22 ± 0.25	3.8 ± 0.8	0.523	−0.118	0.752	−0.385		E,I
210848775	C4	55.615947	20.609693	16.08	0.44 ± 0.08	4054 ± 217	-0.19 ± 0.2	4.8 ± 0.06	0.666	0.223	−0.119	0.061		E
210931967	C4	59.771022	21.895214	15.44	0.26 ± 0.05	3625 ± 197	-0.19 ± 0.28	5 ± 0.07	0.53	0.772	−0.694	0.209		E
211305568	C5	133.122327	9.962734	13.85	0.45 ± 0.03	3612 ± 84	-0.18 ± 0.09	4.8 ± 0.06	0.524	0.699	−0.551	0.148		Dr17
211336288	C5	133.423618	10.564473	14.61	0.59 ± 0.03	3996 ± 79	-0.075 ± 0.084	4.7 ± 0.03	0.591	0.266	−0.056	0.030		Dr17
211357309	C5	133.23263	10.944721	13.15	0.46 ± 0.03	4240 ± 223	-1 ± 0	4.6 ± 0.1	0.674	0.074	0.042	0.014		M,Dr17
211562654	C5	125.00716	14.019461	12.75	0.87 ± 0.04	5482 ± 50	0.09 ± 0.08	4.6 ± 0.1	0.597	−0.275	0.889	−0.429	K2-183	M18
211566738	C5	128.32327	14.078237	14.93	0.47 ± 0.05	4091 ± 155	-0.009 ± 0.16	4.8 ± 0.04	0.59	0.144	0.135	−0.037		E
211828293	C5	123.468508	17.718615	14.71	0.3 ± 0.05	3647 ± 87	0.017 ± 0.1	5 ± 0.06	0.472	0.725	−0.501	0.118		E
212092746	C5	127.644804	21.881783	16.16	0.3 ± 0.04	3669 ± 114	0.013 ± 0.15	5 ± 0.03	0.477	0.733	−0.527	0.13		E
212157262	C5	132.523609	23.192601	12.86	0.83 ± 0.11	5438 ± 63	0 ± 0.1	4.6 ± 0.08	0.584	−0.268	0.901	−0.438	K2-187	M
212303338	C6	202.9588318	−17.4307041	9.96	0.8 ± 0.05	5148 ± 155	0.005 ± 0.1	4.6 ± 0.03	0.626	−0.487	1.19	−0.528		E
212425103	C6	204.3695831	−14.3488894	14.49	0.83 ± 0.06	5490 ± 133	-0.19 ± 0.25	4.5 ± 0.06	0.507	−0.029	0.622	−0.342		E,K19
212443973	C6	205.0088959	−13.9320383	14.95	0.34 ± 0.03	3423 ± 84	0.2 ± 0.084	4.9 ± 0.1	0.496	0.415	−0.004	−0.081		Dr17

Table 1
(Continued)

Candidate	C.	R.A.	Decl.	$m_{\rm Kep}$	$R_\star$ ($R_\odot$)	$T_{\rm eff}$	[Fe/H]	log(g)	u_1[a]	u_2	u_3	u_4	Name	Source[b]
212470904	C6	205.8204651	−13.3571358	13.02	0.72 ± 0.04	4820 ± 124	0.18 ± 0.08	4.6 ± 0.2	0.685	−0.71	1.41	−0.557		M
212532636	C6	205.7254181	−12.0385857	14.05	0.59 ± 0.04	4485 ± 73	−0.3 ± 0.15	4.7 ± 0.04	0.62	−0.531	1.2	−0.465		E
212610063	C6	207.1204529	−10.3622961	14.36	0.77 ± 0.09	5146 ± 185	−0.19 ± 0.3	4.6 ± 0.06	0.575	−0.358	1.07	−0.498		E
212624936	C6	210.6377716	−10.0237617	13.87	0.93 ± 0.2	5765 ± 170	−0.39 ± 0.25	4.4 ± 0.07	0.347	0.576	−0.186	−0.023		E
213715787	C7	293.8331909	−28.4978333	13.36	0.31 ± 0.08	3775 ± 186	−0.1 ± 0.15	5 ± 0.07	0.528	0.76	−0.698	0.222	K2-147	E
214189767	C7	285.0127869	−27.1352367	15.42	0.53 ± 0.04	4148 ± 123	0.043 ± 0.16	4.8 ± 0.03	0.595	−0.051	0.432	−0.138		E
214539781	C7	287.9277344	−26.2420712	14.63	0.41 ± 0.04	3856 ± 122	0.071 ± 0.12	4.9 ± 0.03	0.531	0.431	−0.166	0.024		E
219752140	C7	288.7794495	−15.9167862	12.55	$1^{+0.24}_{-0.12}$	5708 ± 111	−0.068 ± 0.15	4.2 ± 0.2	0.479	0.161	0.322	−0.215		E,I
220250254	C8	17.6409359	1.578266	11.51	0.89 ± 0.15	5500 ± 45	0 ± 0.02	4.6 ± 0.07	0.573	−0.217	0.834	−0.416	K2-210	M
220256496	C8	21.1059532	1.704954	12.87	0.79 ± 0.08	5360 ± 51	−0.04 ± 0.03	4.7 ± 0.06	0.579	−0.281	0.933	−0.449	K2-211	M
220272424	C8	10.5750151	2.048125	13.84	0.52 ± 0.07	4183 ± 128	−0.044 ± 0.15	4.8 ± 0.05	0.61	−0.057	0.408	−0.124		E
220383386	C8	8.7396841	4.3814678	8.95	0.83 ± 0.03	5438 ± 63	−0.1 ± 0.1	4.6 ± 0.1	0.542	−0.137	0.748	−0.383	HD 3167	M,V16
220440058	C8	15.725172	5.4905128	16.27	0.28 ± 0.08	3682 ± 217	−0.18 ± 0.25	5 ± 0.07	0.544	0.774	−0.734	0.232		E
220492298	C8	16.7614613	6.588829	13.79	0.89 ± 0.09	5620 ± 31	0.28 ± 0.03	4.5 ± 0.08	0.629	−0.309	0.887	−0.422		M
220554126	C8	15.5148172	7.9936891	15.79	0.45 ± 0.06	4073 ± 201	−0.19 ± 0.2	4.8 ± 0.06	0.658	0.186	−0.049	0.037		E
220554210	C8	13.4320173	7.995316	13.72	1 ± 0.04	5499 ± 109	−0.23 ± 0.16	4.5 ± 0.04	0.49	0.025	0.561	−0.321	K2-282	H16,K19
220674823	C8	13.0797796	10.7946987	11.96	0.95 ± 0.05	5613 ± 39	0.01 ± 0.01	4.6 ± 0.07	0.549	−0.104	0.673	−0.354	K2-106	M,S17
220687583	C8	16.4097919	11.1298952	13.64	0.81 ± 0.04	5259 ± 148	−0.15 ± 0.16	4.5 ± 0.04	0.565	−0.278	0.956	−0.46		E,I
228721452	C10	185.306152	−10.282037	11.32	1 ± 0.06	5859 ± 50	0.19 ± 0.08	4.5 ± 0.1	0.55	−0.001	0.48	−0.272	K2-223	M18
228732031	C10	182.751564	−9.765218	11.94	0.81 ± 0.03	5200 ± 100	−0.02 ± 0.08	4.6 ± 0.1	0.612	−0.43	1.13	−0.511	K2-131	Da17
228739208	C10	188.441461	−9.419237	12.11	1 ± 0.26	5791 ± 139	−0.21 ± 0.32	4.4 ± 0.2	0.413	0.372	0.062	−0.118		E
228801451	C10	186.873264	−6.721861	10.96	0.79 ± 0.01	5315 ± 35	−0.09 ± 0.02	4.6 ± 0.01	0.568	−0.26	0.916	−0.443	K2-229	L18
228813918	C10	186.870725	−6.195224	14.53	0.29 ± 0.06	3697 ± 109	−0.059 ± 0.18	5 ± 0.06	0.493	0.788	−0.66	0.191	K2-137	H16
228814754	C10	186.267537	−6.162735	14.57	0.21 ± 0.09	3521 ± 467	−0.22 ± 0.6	5.1 ± 0.1	0.503	0.781	−0.64	0.174		E
228836835	C10	189.575383	−5.244647	14.93	0.32 ± 0.07	3782 ± 152	−0.18 ± 0.25	5 ± 0.07	0.576	0.714	−0.712	0.238		E
228877886	C10	186.533953	−3.65254	14.37	0.73 ± 0.04	4837 ± 117	−0.18 ± 0.35	4.6 ± 2	0.619	−0.578	1.34	−0.566		E,I

Notes.

[a] u_1, u_2, u_3, u_4: limb-darkening parameters from Claret & Bloemen (2011).

[b] Source of stellar parameter values: E = used EPIC parameters; M = $T_{\rm eff}$, log(g), and [Fe/H] from McDonald observations; I = $R_\star$ calculated using isochrones from Dotter et al. (2008); B = $R_\star$ calculated using relations from Boyajian et al. (2012); M13 = Mortier et al. (2013); B15 = Becker et al. (2015); H16 = Huber et al. (2016); V16 = Vanderburg et al. (2016a); Da17 = Dai et al. (2017); Dr17 = Dressing et al. (2017); S17 = Sinukoff et al. (2017); M18 = Mayo et al. (2018); Dr19 = Dressing et al. (2019); K19 = Kruse et al. (2019); P = inferred from photometry using Pinsonneault et al. (2012); see Section 6.1.1.

(This table is available in its entirety in machine-readable form.)

Table 2
Transit Model Fit Results

EPIC	Pl.[a]	Period (days)	T_0 (HJD-2,450,000)	R_p/R_*	$R_p(R_\oplus)$	a/R_*	$i(^\circ)$	Ind. FPP	FPP	S/N	Status[b]	Prior[c]
201085153	p1	0.25722 ± 0.000029	$7627.05811^{+0.00094}_{-0.00083}$	$0.0584^{+0.004}_{-0.0024}$	2.5 ± 1	$2.4^{+0.3}_{-0.4}$	90.7^{+20}_{-10}	0.11	0.11	26		
201085153	p2	2.259796 ± 0.00026	$7642.94739^{+0.011}_{-0.017}$	$0.0341^{+0.0041}_{-0.0055}$	1.3 ± 0.6	9	90	0.13	0.0087	4.1		
201089381	p1	0.160419 ± 0.0000083	7604.12593 ± 0.00027	$0.033^{+0.0013}_{-0.00077}$	2.8 ± 0.5	$2.8^{+0.1}_{-0.3}$	91.7^{+10}_{-9}	NA[d]	⋯	40		
201110617	p1	0.813143 ± 0.000077	$7641.67248^{+0.0014}_{-0.0012}$	$0.0162^{+0.0013}_{-0.0006}$	$1.1^{+0.09}_{-0.06}$	$4.4^{+0.4}_{-0.8}$	89.8^{+8}_{-7}	1.6e−8	1.6e−8	26	Conf.	Dr17
201130233	p1	0.365261 ± 0.00017	$7638.7224^{+0.0021}_{-0.0019}$	$0.0107^{+0.0011}_{-0.00063}$	$1^{+0.1}_{-0.08}$	2.2 ± 0.4	89.7 ± 20	0.0046	0.0046	15	Conf.	M18
201214691	p1	0.600446 ± 0.000068	$6880.68578^{+0.0034}_{-0.0029}$	$0.0112^{+0.0016}_{-0.00098}$	0.97 ± 0.1	$3.3^{+0.9}_{-0.7}$	91.1 ± 10	0.035	0.035	9.5		
201230694	p1	0.273413 ± 0.000061	$6853.61225^{+0.0018}_{-0.0016}$	$0.0212^{+0.0024}_{-0.0012}$	1.1 ± 0.1	$2.2^{+0.6}_{-0.4}$	91.5 ± 20	0.067	0.067	16		
201231940	p1	0.57309 ± 0.000045	$6862.0756^{+0.0016}_{-0.0014}$	$0.0691^{+0.025}_{-0.0062}$	$2.3^{+0.6}_{-0.4}$	5.8^{+7}_{-2}	90.2^{+6}_{-5}	0.76	0.76	14		V16a
201239401	p1	0.905626 ± 0.00002	$6811.84172^{+0.0015}_{-0.0013}$	$0.0239^{+0.0017}_{-0.00087}$	0.88 ± 0.2	$5.2^{+0.6}_{-1}$	89.3^{+9}_{-7}	0.53	0.53	24		V16a
201239401	p2	6.783592 ± 0.00019	$6863.39748^{+0.0089}_{-0.0059}$	$0.0207^{+0.003}_{-0.002}$	0.77 ± 0.2	19 ± 6	90.3 ± 2	0.77	0.051	5.8		
201264302	p1	0.212203 ± 0.0000078	$6828.10358^{+0.00041}_{-0.00041}$	$0.0233^{+0.0015}_{-0.00055}$	$0.49^{+0.03}_{-0.02}$	$3^{+0.3}_{-0.4}$	91.2^{+10}_{-9}	0.13	0.13	39		V16a
201427007	p1	0.72091 ± 0.00014	$7625.7943^{+0.0027}_{-0.0023}$	$0.0142^{+0.0013}_{-0.00067}$	1.5 ± 0.2	$3.1^{+0.3}_{-0.6}$	88.5 ± 10	0.00024	0.00024	16	Conf.	
201438507	p1	0.326564 ± 0.000034	$7611.32309^{+0.0014}_{-0.0013}$	$0.0145^{+0.0038}_{-0.00096}$	$1.5^{+0.4}_{-0.3}$	$3.5^{+3}_{-0.8}$	89.3^{+10}_{-7}	0.46	0.46	13		
201438507	p2	2.536236 ± 0.00031	$7609.54335^{+0.0065}_{-0.0074}$	$0.0112^{+0.0017}_{-0.0019}$	1.1 ± 0.2	16	90	0.5	0.033	3.4		
201461352	p1	0.696099 ± 0.000057	$6858.64842^{+0.0029}_{-0.002}$	$0.0331^{+0.011}_{-0.0036}$	$0.59^{+0.2}_{-0.09}$	5.9^{+6}_{-2}	90.1^{+6}_{-5}	0.85	0.85	8.7		
201469738	p1	0.276097 ± 0.000052	$6830.54448^{+0.0016}_{-0.0024}$	$0.0167^{+0.016}_{-0.0013}$	$1.2^{+0.7}_{-0.4}$	$2.6^{+10}_{-0.6}$	90^{+9}_{-6}	0.67	0.67	7.2		
201549425	p1	0.383255 ± 0.000052	$6865.80605^{+0.0033}_{-0.0022}$	$0.0155^{+0.0069}_{-0.0016}$	$0.96^{+0.4}_{-0.2}$	$3.1^{+5}_{-0.6}$	89.8^{+9}_{-7}	0.39	0.39	8.9		
201595106	p1	0.877214 ± 0.00006	$7608.48962^{+0.0014}_{-0.0012}$	$0.0126^{+0.00098}_{-0.00036}$	1.3 ± 0.1	$5.8^{+0.7}_{-1}$	89.2^{+8}_{-5}	0.0076	0.0076	24	Conf.	M18
201609593	p1	0.318254 ± 0.000041	$6814.04212^{+0.0022}_{-0.0019}$	$0.0138^{+0.0068}_{-0.0016}$	$0.5^{+0.2}_{-0.1}$	$3^{+5}_{-0.7}$	89.6^{+9}_{-7}	0.72	0.72	8.9		
201609593	p2	1.392535 ± 0.00053	$6856.48324^{+0.0066}_{-0.0075}$	$0.011^{+0.0015}_{-0.0019}$	$0.34^{+0.05}_{-0.07}$	9	90	2.3e−8	2.3e−8	3.8		
201637175	p1	0.381073 ± 0.000024	$6846.94318^{+0.00031}_{-0.00036}$	$0.0366^{+0.0014}_{-0.00083}$	2.3 ± 0.1	$3^{+0.08}_{-0.2}$	90.6^{+8}_{-7}	1	1	37	Conf.	S15
201650711	p1	0.259661 ± 0.000058	$6828.61939^{+0.0012}_{-0.001}$	$0.00824^{+0.00093}_{-0.00056}$	$0.31^{+0.06}_{-0.05}$	$2.9^{+0.7}_{-0.6}$	89 ± 10	0.49	0.49	18		
201650711	p2	5.544059 ± 0.000046	6853.70238 ± 0.004	$0.0106^{+0.0014}_{-0.00068}$	$0.41^{+0.08}_{-0.07}$	20^{+4}_{-5}	90.2 ± 2	0.029	0.0019	9.4		K19
201687804	p1	0.297142 ± 0.000095	$6844.48164^{+0.0023}_{-0.0015}$	$0.00833^{+0.00094}_{-0.00056}$	$0.58^{+0.08}_{-0.07}$	$2.1^{+0.4}_{-0.3}$	89.8 ± 20	0.074	0.074	14		
201717159	p1	0.604066 ± 0.000039	$6813.86171^{+0.0018}_{-0.0016}$	$0.0261^{+0.0028}_{-0.0014}$	1.3 ± 0.2	$4.3^{+0.9}_{-1}$	90.5^{+10}_{-9}	0.024	0.024	17		V16a
201796374	p1	0.412222 ± 0.000045	6844.67348 ± 0.0012	$0.0338^{+0.011}_{-0.0027}$	$1^{+0.3}_{-0.2}$	5.5^{+6}_{-1}	89.7 ± 5	0.29	0.29	16		
201923289	p1	0.782113 ± 0.000033	$6861.99499^{+0.0025}_{-0.0022}$	$0.0128^{+0.0013}_{-0.00066}$	1.2 ± 0.1	$4^{+0.7}_{-0.9}$	91.5 ± 10	0.054	0.054	16		V16a
203533312	p1	0.175661 ± 0.00002	6964.02466 ± 0.00025	$0.0237^{+0.00056}_{-0.0002}$	3.5 ± 0.3	$1.6^{+0.04}_{-0.09}$	89.6^{+20}_{-9}	NA[d]	⋯	54		A16
205002291	p1	0.857941 ± 0.000092	$6895.58103^{+0.0024}_{-0.0013}$	$0.0241^{+0.0026}_{-0.0013}$	0.83 ± 0.2	6 ± 1	90.6 ± 7	0.97	0.97	16	FP	
205152172	p1	0.980088 ± 0.000061	$6895.59262^{+0.0011}_{-0.00092}$	$0.02^{+0.0016}_{-0.00053}$	1.2 ± 0.2	$6.6^{+0.5}_{-1}$	89.6 ± 5	0.24	0.24	28		V16a
205152172	p2	3.224517 ± 0.00028	$6931.20494^{+0.0022}_{-0.0025}$	$0.0166^{+0.0028}_{-0.0014}$	0.99 ± 0.2	25^{+10}_{-7}	90^{+2}_{-1}	0.25	0.017	10		
206024342	p1	0.911724 ± 0.000076	$7016.52991^{+0.0027}_{-0.0018}$	$0.0117^{+0.0011}_{-0.00056}$	1.4 ± 0.5	$4.7^{+0.7}_{-1}$	91.7 ± 9	6.5e−5	4.4e−6	11	Conf.	V16a
206024342	p2	4.508035 ± 0.00042	$7033.78077^{+0.0033}_{-0.0025}$	$0.0149^{+0.0014}_{-0.00086}$	1.7 ± 0.6	17^{+2}_{-4}	89.8^{+3}_{-2}	0.0063	0.00042	12	Conf.	V16a
206024342	p3	14.647531 ± 0.0000041	$6985.47506^{+0.0038}_{-0.0025}$	$0.0217^{+0.0016}_{-0.00073}$	2.6 ± 0.9	29^{+2}_{-6}	90^{+2}_{-1}	1.9e−6	1.9e−6	15	Conf.	K19
206024342	p4	27.718603 ± 0.1	$7017.0414^{+0.039}_{-0.018}$	$0.0111^{+0.0023}_{-0.0015}$	1.3 ± 0.5	28^{+10}_{-9}	90^{+2}_{-1}	6.8e−5	4.6e−6	3.6	Conf.	
206042996	p1	0.354884 ± 0.000063	$7007.06827^{+0.002}_{-0.0017}$	$0.0223^{+0.0026}_{-0.0013}$	$1.2^{+0.2}_{-0.1}$	2.6 ± 0.5	89.9^{+20}_{-10}	0.029	0.0019	14	Conf.	V16a
206042996	p2	5.2986 ± 0.0006	$6989.0462^{+0.0053}_{-0.0047}$	$0.0303^{+0.0041}_{-0.0025}$	1.7 ± 0.2	16^{+3}_{-4}	90.5 ± 3	0.015	0.00098	12	Conf.	K19
206103150	p1	0.789655 ± 0.00004	$6990.82197^{+0.0013}_{-0.00097}$	$0.0139^{+0.00076}_{-0.00034}$	$1.8^{+0.1}_{-0.09}$	$3.2^{+0.2}_{-0.4}$	89.6^{+10}_{-9}	1.2e−7	8e−9	20	Conf.	B15
206103150	p2	9.028052 ± 0.000065	$6997.34398^{+0.0013}_{-0.00088}$	$0.026^{+0.00072}_{-0.00033}$	3.3 ± 0.1	$17^{+0.3}_{-1}$	$89.5^{+2}_{-0.9}$	0.00013	8.5e − 6	39	Conf.	B15
206151047	p1	0.358442 ± 0.0000085	$7015.6764^{+0.0013}_{-0.00087}$	$0.0138^{+0.0021}_{-0.00076}$	1.9 ± 0.9	$4.4^{+2}_{-0.9}$	91 ± 8	0.57	0.57	18		V16a
206215704	p1	0.623232 ± 0.00003	$7039.60634^{+0.0014}_{-0.0012}$	$0.0346^{+0.0051}_{-0.0025}$	0.96 ± 0.1	7.3^{+3}_{-2}	90.1^{+6}_{-4}	0.44	0.018	14	Conf.	V16a
206215704	p2	2.255436 ± 0.000091	$7010.0072^{+0.0018}_{-0.0016}$	$0.0383^{+0.0036}_{-0.0024}$	$1^{+0.1}_{-0.09}$	17^{+3}_{-4}	89.9^{+3}_{-2}	0.085	0.0034	13	Conf.	K19
206215704	p3	2.909219 ± 0.000035	$7043.29037^{+0.0019}_{-0.0017}$	$0.0398^{+0.0051}_{-0.0025}$	1.1 ± 0.1	24 ± 7	90 ± 2	0.27	0.011	12	Conf.	

Table 2
(Continued)

EPIC	Pl.[a]	Period (days)	T_0 (HJD-2,450,000)	R_p/R_*	$R_p(R_\oplus)$	a/R_*	$i(^\circ)$	Ind. FPP	FPP	S/N	Status[b]	Prior[c]
206298289	p1	0.434847 ± 0.000046	$6987.59112^{+0.00089}_{-0.00078}$	$0.0247^{+0.0016}_{-0.00094}$	$0.89^{+0.1}_{-0.09}$	$4.2^{+0.4}_{-0.8}$	88.5^{+10}_{-7}	0.037	0.037	26		V16a
206298289	p2	3.215738 ± 0.000078	$6992.50972^{+0.0032}_{-0.0028}$	$0.0232^{+0.0028}_{-0.0018}$	0.85 ± 0.1	20^{+5}_{-6}	90 ± 2	0.41	0.027	7.8		
206417197	p1	0.442112 ± 0.000039	$7022.51794^{+0.0014}_{-0.0016}$	$0.0133^{+0.0013}_{-0.00059}$	$1.1^{+0.1}_{-0.09}$	$3^{+0.4}_{-0.6}$	88.5^{+10}_{-9}	0.11	0.11	19		V16a
210605073	p1	0.567003 ± 0.000025	$7130.83584^{+0.00059}_{-0.00052}$	$0.0903^{+0.0047}_{-0.0021}$	16^{+4}_{-3}	$5.2^{+0.3}_{-0.9}$	90.2^{+8}_{-7}	0.72	0.72	39		A16
210707130	p1	0.684559 ± 0.00001	$7102.33296^{+0.00056}_{-0.00042}$	$0.0155^{+0.00088}_{-0.00032}$	$1.2^{+0.08}_{-0.07}$	$6.1^{+0.4}_{-0.7}$	89.4^{+6}_{-4}	0.00017	0.00017	37	Conf.	Dr17
210801536	p1	0.892592 ± 0.000036	$7130.80967^{+0.0037}_{-0.0025}$	$0.0105^{+0.0012}_{-0.0008}$	$1^{+0.3}_{-0.2}$	$4.3^{+0.8}_{-1}$	90.8^{+10}_{-8}	0.026	0.026	9.6		K19
210801536	p2	5.044155 ± 0.00022	$7102.84382^{+0.0094}_{-0.0063}$	$0.0126^{+0.002}_{-0.0017}$	$1.2^{+0.4}_{-0.2}$	16^{+8}_{-5}	90.2^{+3}_{-2}	0.39	0.39	4.4		
210848775	p1	0.214079 ± 0.00003	$7104.33168^{+0.0018}_{-0.0015}$	$0.0224^{+0.0031}_{-0.0021}$	$1.1^{+0.3}_{-0.2}$	$2.2^{+0.9}_{-0.4}$	90.8^{+20}_{-10}	0.28	0.28	11		
210931967	p1	0.346547 ± 0.000042	$7124.31547^{+0.0012}_{-0.0011}$	$0.0232^{+0.006}_{-0.0015}$	0.71 ± 0.2	4.9^{+4}_{-1}	89.3^{+7}_{-5}	0.68	0.68	18		
211305568	p1	$0.197843 \pm 9.4e-5$	$7173.01294^{+0.0011}_{-0.00084}$	$0.0134^{+0.0014}_{-0.00072}$	$0.67^{+0.08}_{-0.07}$	$2.1^{+0.6}_{-0.4}$	91.6^{+20}_{-10}	0.59	0.59	15		Dr17
211305568	p2	11.54962	$7203.98574^{+0.0021}_{-0.0032}$	$0.0306^{+0.0063}_{-0.0042}$	$1.5^{+0.3}_{-0.2}$	72^{+50}_{-30}	$90.1^{+0.6}_{-0.5}$	1	0.067	4.6		Dr17
211336288	p1	0.221814 ± 0.000062	$7143.81329^{+0.0021}_{-0.0014}$	$0.0147^{+0.0039}_{-0.0011}$	$0.98^{+0.2}_{-0.1}$	$2.1^{+2}_{-0.4}$	89.4^{+20}_{-10}	0.78	0.78	12		Dr17
211357309	p1	0.463974 ± 0.0000011	$7189.86394^{+0.0009}_{-0.00079}$	$0.0159^{+0.0011}_{-0.00055}$	0.81 ± 0.07	$4.3^{+0.5}_{-0.7}$	90.7^{+9}_{-7}	0.36	0.36	26		A16
211357309	p2	11.623464 ± 0.0000039	$7174.22919^{+0.0015}_{-0.0013}$	$0.0248^{+0.0028}_{-0.0014}$	$1.3^{+0.2}_{-0.1}$	98^{+20}_{-30}	90 ± 0.4	0.32	0.021	8.8		
211562654	p1	0.469285 ± 0.000064	$7196.91237^{+0.0019}_{-0.0017}$	$0.0117^{+0.00098}_{-0.00049}$	$1.1^{+0.1}_{-0.08}$	$2.5^{+0.3}_{-0.4}$	90.1^{+20}_{-10}	0.00042	2.8e−5	13	Conf.	M18
211562654	p2	10.787992 ± 0.00033	$7212.47321^{+0.0026}_{-0.0023}$	$0.0242^{+0.0014}_{-0.00065}$	$2.3^{+0.2}_{-0.1}$	22^{+1}_{-3}	90.5 ± 2	0.025	0.0017	18	Conf.	M18
211562654	p3	22.620344 ± 0.000067	7212.0276 ± 0.0036	$0.0244^{+0.0021}_{-0.0011}$	2.3 ± 0.2	49^{+5}_{-10}	$89.9^{+0.8}_{-0.7}$	0.028	0.0011	11	Conf.	M18
211566738	p1	0.760983 ± 0.00004	$7206.50131^{+0.0021}_{-0.0016}$	$0.0198^{+0.0028}_{-0.0014}$	$1.1^{+0.2}_{-0.1}$	5.7^{+2}_{-1}	89.9^{+7}_{-6}	0.35	0.35	14		
211828293	p1	0.699739 ± 0.000035	7211.67533 ± 0.0015	$0.0303^{+0.015}_{-0.0041}$	$1.2^{+0.4}_{-0.3}$	8.8^{+20}_{-1}	89.9^{+3}_{-2}	0.48	0.48	12		
212092746	p1	0.562193 ± 0.000034	$7158.44518^{+0.0013}_{-0.0011}$	$0.0375^{+0.0082}_{-0.0049}$	$1.2^{+0.3}_{-0.2}$	7.8^{+6}_{-2}	90.1^{+5}_{-4}	0.48	0.48	14		
212157262	p1	0.77401 ± 0.000083	$7184.43637^{+0.0016}_{-0.0018}$	$0.0132^{+0.0011}_{-0.00053}$	1.2 ± 0.2	$3.9^{+0.4}_{-0.8}$	89.7^{+10}_{-8}	1.5e−6	5.8e−8	14	Conf.	M18
212157262	p2	2.871512 ± 0.00012	$7144.63842^{+0.0027}_{-0.0024}$	$0.0154^{+0.0015}_{-0.00067}$	1.4 ± 0.2	$9.2^{+0.8}_{-2}$	90.4^{+5}_{-4}	0.00034	1.4e−5	14	Conf.	M18
212157262	p3	7.149584 ± 0.00012	$7203.52085^{+0.0019}_{-0.0013}$	$0.0259^{+0.0015}_{-0.00069}$	2.4 ± 0.3	$18^{+0.9}_{-3}$	90.3^{+2}_{-1}	3.6e−5	1.4e−6	19	Conf.	M18
212157262	p4	13.606629 ± 0.0000036	$7155.08495^{+0.0031}_{-0.0027}$	$0.0206^{+0.0017}_{-0.00077}$	1.9 ± 0.3	28^{+2}_{-6}	90.1^{+1}_{-2}	1.6e − 11	6.5e − 13	13	Conf.	M18
212303338	p1	0.595491 ± 0.000055	$7264.23209^{+0.0028}_{-0.0025}$	$0.00539^{+0.00073}_{-0.00048}$	$0.47^{+0.07}_{-0.06}$	4 ± 1	89.4^{+10}_{-9}	0.8	0.8	9		M18
212425103	p1	0.945974 ± 0.000011	7226.68722 ± 0.0019	$0.0172^{+0.0016}_{-0.00078}$	$1.6^{+0.2}_{-0.1}$	$4.9^{+0.6}_{-1}$	90.2^{+9}_{-8}	0.012	0.012	18		K19
212443973	p1	0.779407 ± 0.000014	$7239.5629^{+0.0021}_{-0.0019}$	$0.018^{+0.0048}_{-0.0013}$	$0.73^{+0.2}_{-0.1}$	7.4^{+6}_{-2}	90.9 ± 5	0.59	0.59	9.2		Dr17
212470904	p1	0.642926 ± 0.000019	$7280.92925^{+0.0019}_{-0.0014}$	$0.0115^{+0.0015}_{-0.00093}$	$0.91^{+0.1}_{-0.09}$	5.5^{+2}_{-1}	89.6^{+7}_{-6}	0.16	0.16	14		
212532636	p1	0.314842 ± 0.000024	$7242.75694^{+0.0013}_{-0.0015}$	$0.0132^{+0.0018}_{-0.00081}$	$0.88^{+0.1}_{-0.09}$	$2.9^{+0.7}_{-0.6}$	89.7 ± 10	0.078	0.078	18		
212610063	p1	0.43514 ± 0.000049	$7272.1437^{+0.0021}_{-0.0018}$	$0.0131^{+0.0014}_{-0.00093}$	1.1 ± 0.2	3 ± 0.6	88.1^{+20}_{-10}	0.037	0.037	13		
212624936	p1	0.578657 ± 0.000016	$7232.53108^{+0.0025}_{-0.0022}$	$0.0114^{+0.0011}_{-0.00071}$	1.2 ± 0.3	$3^{+0.4}_{-0.6}$	90.3 ± 10	0.0041	0.0041	13	Conf.	
212624936	p2	11.811437 ± 0.00011	$7233.78707^{+0.0029}_{-0.0033}$	$0.0226^{+0.0022}_{-0.0011}$	2.3 ± 0.5	41^{+5}_{-10}	$90^{+1}_{-0.9}$	0.048	0.0032	10	Conf.	
213715787	p1	0.961918 ± 0.000013	$7327.91683^{+0.00089}_{-0.001}$	$0.0213^{+0.0014}_{-0.00072}$	0.73 ± 0.2	$7.9^{+0.8}_{-2}$	89.9^{+5}_{-4}	2.7e − 5	2.7e − 5	25	Conf.	H18
214189767	p1	0.520638 ± 0.000091	$7327.11571^{+0.0033}_{-0.0028}$	$0.0205^{+0.0026}_{-0.0017}$	$1.2^{+0.2}_{-0.1}$	$3.1^{+0.9}_{-0.7}$	90.6 ± 10	0.93	0.93	8		
214539781	p1	0.437366 ± 0.000039	$7309.36511^{+0.0014}_{-0.0016}$	$0.0169^{+0.0023}_{-0.0011}$	0.78 ± 0.1	$4.1^{+2}_{-0.9}$	89.4^{+10}_{-7}	0.97	0.97	15	FP	
219752140	p1	0.877836 ± 0.00021	$7371.26939^{+0.0048}_{-0.0037}$	$0.0104^{+0.0015}_{-0.00099}$	$1.2^{+0.3}_{-0.2}$	4.6^{+2}_{-1}	89.5^{+10}_{-8}	0.96	0.96	7.9		
220250254	p1	0.57023 ± 0.000032	$7465.80382^{+0.0023}_{-0.0012}$	$0.00874^{+0.001}_{-0.00061}$	0.86 ± 0.2	4.4 ± 1	89.2^{+10}_{-8}	0.036	0.036	16	Conf.	M18
220256496	p1	0.669532 ± 0.000019	7395.82322 ± 0.0016	$0.0149^{+0.0013}_{-0.00048}$	1.3 ± 0.2	$3.7^{+0.5}_{-0.8}$	89.6 ± 10	0.0029	0.0029	21	Conf.	M18
220256496	p2	2.601267 ± 0.00014	7470.75432 ± 0.0033	$0.0145^{+0.0018}_{-0.00091}$	1.3 ± 0.2	11^{+2}_{-3}	89.8^{+4}_{-3}	0.0064	0.00043	8.7	Conf.	
220272424	p1	0.659967 ± 0.000064	$7452.27858^{+0.0023}_{-0.0017}$	$0.0145^{+0.0022}_{-0.0011}$	$0.85^{+0.2}_{-0.1}$	5.1^{+2}_{-1}	89.5^{+9}_{-7}	0.2	0.2	9.3		
220383386	p1	0.959622 ± 0.000044	$7410.69248^{+0.001}_{-0.00091}$	$0.0171^{+0.00092}_{-0.00042}$	$1.6^{+0.09}_{-0.08}$	$4.7^{+0.2}_{-0.7}$	90.2^{+7}_{-6}	0.0003	2e − 5	21	Conf.	V16b
220383386	p2	29.875221 ± 0.0004	$7454.69902^{+0.0038}_{-0.0033}$	$0.0251^{+0.0017}_{-0.00087}$	$2.3^{+0.2}_{-0.1}$	39^{+2}_{-6}	$90^{+0.9}_{-0.8}$	0.14	0.0095	14	Conf.	V16b
220440058	p1	0.626683 ± 0.000026	$7428.38519^{+0.0019}_{-0.0013}$	$0.0442^{+0.0049}_{-0.0025}$	1.4 ± 0.4	5.2 ± 1	89.4^{+9}_{-7}	0.06	0.06	17		

Table 2
(Continued)

EPIC	Pl.[a]	Period (days)	T_0 (HJD-2,450,000)	R_p/R_*	$R_p(R_\oplus)$	a/R_*	$i(^\circ)$	Ind. FPP	FPP	S/N	Status[b]	Prior[c]
220440058	p2	3.835187 ± 0.000098	$7401.85905^{+0.0027}_{-0.0024}$	$0.053^{+0.014}_{-0.0057}$	$1.7^{+0.6}_{-0.5}$	39	$88.9^{+2}_{-0.2}$	0.64	0.043	7		
220492298	p1	0.762406 ± 0.00015	$7431.67734^{+0.0037}_{-0.0033}$	$0.01^{+0.0012}_{-0.00072}$	0.99 ± 0.1	$3.2^{+0.6}_{-0.7}$	92.6 ± 10	0.00069	0.00069	11	Conf.	
220554126	p1	0.412326 ± 0.00007	$7430.58836^{+0.0033}_{-0.0029}$	$0.0161^{+0.0021}_{-0.0014}$	0.8 ± 0.1	$2.5^{+0.7}_{-0.5}$	90.7^{+20}_{-10}	0.098	0.098	8.8		
220554210	p1	0.70531 ± 0.000037	$7466.1131^{+0.0019}_{-0.0022}$	$0.0145^{+0.0011}_{-0.00065}$	1.6 ± 0.1	$3^{+0.3}_{-0.5}$	91.3 ± 10	1.1e − 9	7.5e − 11	21	Conf.	
220554210	p2	4.169783 ± 0.000089	$7457.54493^{+0.0025}_{-0.0022}$	$0.0227^{+0.0016}_{-0.00073}$	$2.5^{+0.2}_{-0.1}$	$11^{+0.8}_{-2}$	90.1^{+4}_{-3}	1.8e − 7	1.2e − 8	18	Conf.	K19
220554210	p3	27.263595 ± 0.0009	$7426.94269^{+0.01}_{-0.0052}$	$0.0233^{+0.003}_{-0.0014}$	$2.6^{+0.3}_{-0.2}$	42^{+5}_{-10}	90.1 ± 1	0.00013	5.4e − 6	8.6	Conf.	
220674823	p1	0.571212 ± 0.000038	$7417.43601^{+0.00091}_{-0.00079}$	$0.0157^{+0.00069}_{-0.00031}$	1.6 ± 0.1	$2.9^{+0.1}_{-0.3}$	89.7 ± 10	6.3e − 5	4.2e − 6	36	Conf.	A17
220674823	p2	13.334615 ± 0.0001	$7405.70999^{+0.0028}_{-0.0032}$	$0.0209^{+0.0015}_{-0.00055}$	2.2 ± 0.2	26^{+2}_{-5}	90.2 ± 1	5.4e − 8	3.6e − 9	19	Conf.	A17
220687583	p1	0.45693 ± 0.000073	$7466.50516^{+0.0023}_{-0.002}$	$0.013^{+0.0017}_{-0.00087}$	1.2 ± 0.1	$3.4^{+0.9}_{-0.8}$	89.2 ± 10	0.013	0.013	11		
228721452	p1	0.50557 ± 0.000088	$7637.66396^{+0.0023}_{-0.002}$	$0.00801^{+0.0008}_{-0.00053}$	$0.89^{+0.1}_{-0.09}$	$3.3^{+0.8}_{-0.7}$	89.7 ± 10	0.029	0.0019	10	Conf.	
228721452	p2	4.562546 ± 0.00014	$7628.61208^{+0.0029}_{-0.0025}$	$0.0129^{+0.0012}_{-0.00042}$	1.5 ± 0.1	13^{+1}_{-3}	89.6^{+4}_{-3}	0.0025	0.0025	15	Conf.	M18
228732031	p1	0.369311 ± 0.00003	$7605.09575^{+0.00091}_{-0.00025}$	$0.0172^{+0.00041}_{-0.00027}$	$1.5^{+0.07}_{-0.06}$	3 ± 0.2	89.7^{+7}_{-6}	0.45	0.45	32	Conf.	Da17
228739208	p1	0.483787 ± 0.000033	$7607.43487^{+0.0021}_{-0.0019}$	$0.00918^{+0.004}_{-0.001}$	$1.1^{+0.5}_{-0.3}$	$4.2^{+7}_{-0.9}$	90.8^{+7}_{-6}	0.99	0.99	9.5		
228801451	p1	0.584216 ± 0.000022	$7646.56655^{+0.00046}_{-0.00077}$	$0.0118^{+0.00023}_{-0.0002}$	1 ± 0.02	$4.2^{+0.3}_{-0.2}$	89.7 ± 4	0.00012	0.00012	29	Conf.	M18
228813918	p1	0.179719 ± 0.000028	$7639.27571^{+0.00077}_{-0.00068}$	$0.02^{+0.0016}_{-0.00081}$	0.64 ± 0.1	$2.1^{+0.4}_{-0.3}$	93.1^{+10}_{-20}	0.0011	0.0011	25	Conf.	S18
228814754	p1	0.844537 ± 0.000025	$7650.61924^{+0.00071}_{-0.00047}$	$0.0593^{+0.0053}_{-0.0027}$	1.4 ± 0.6	11 ± 2	89.9 ± 3	0.39	0.39	25		
228836835	p1	0.728113 ± 0.000063	$7585.45061^{+0.0014}_{-0.0012}$	$0.0299^{+0.003}_{-0.0018}$	$1.1^{+0.3}_{-0.2}$	6.4^{+1}_{-2}	89.7^{+7}_{-5}	0.0058	0.0058	16	Conf.	
228877886	p1	0.778286 ± 0.00011	$7642.77006^{+0.0038}_{-0.0029}$	$0.0125^{+0.0019}_{-0.0011}$	1 ± 0.1	$3.9^{+0.9}_{-1}$	89.6 ± 10	0.015	0.015	8.7		

Notes.

[a] All known planets in a system are numbered in order of distance from the star and may differ from the b/c/d/e letters assigned to confirmed planets in order of discovery, and from the 01, 02, etc. designations of K2 candidates.

[b] Conf. = statistically validated or confirmed by radial velocity mass measurement here or in prior work. FP = likely false positive. Note that candidates with S/N < 10 are not identified as either confirmed or false positives regardless of FPP.

[c] Candidate or confirmed planet was first noted in a prior paper: B15 = Becker et al. (2015), S15: Sanchis-Ojeda et al. (2015b), V16a = Vanderburg et al. (2016b), V16b = Vanderburg et al. (2016a), A16 = Adams et al. (2016), A17 = Adams et al. (2017), Dr17 = Dressing et al. (2017), Da17 = Dai et al. (2017), M18 = Mayo et al. (2018), H18 = Hirano et al. (2018), S18 = Smith et al. (2018), K19 = Kruse et al. (2019).

[d] See Section 6.1.2.

(This table is available in its entirety in machine-readable form.)

in this paper. Complementary programs to identify nontransiting, longer-period companions are also recommended, such as long-term RV monitoring, through which planets have been found around HD 3167 (Christiansen et al. 2017) and WASP-47 (Neveu-VanMalle et al. 2016). Both projects are, however, well beyond the scope of the present work.

To conduct our search, we first compiled values from the literature for all of the known companions to our 74 USP candidates. For each candidate that has already been identified in the literature, starting with the USP (which we designate p1, to avoid confusion with other designations in the literature), we folded the transit data at the known period and fit for the transit light curve (as in Section 2).

Overlapping transits are common in multiplanet systems, particularly for USPs with frequent transits. We found, however, that the impact of overlapping exterior transits on the parameters derived for the USP is minimal because the fraction of USP transits that are overlapped is typically small. Overlap is more important for the outer planets, particularly those with only a handful of transits. Thus, we subtracted the best-fit model for the USP from the light curve before searching for the next potential candidate planet. For systems with companions that have already been identified, we used the reported orbital periods to progressively search for, fit, and remove each of the companion transit signals. After exhausting the list of known companion periods, we searched for new periodic signals, both between known orbital periods (if there are already multiple candidates identified) and beyond the longest period identified (we formally searched out to half the length of the time series). For simplicity, we used the same EEBLS routine for longer-period planets as we used to search for USPs, which may affect recovery efficiencies, though with a median $P = 4.5$ days, most companions have short-enough transit durations that the 1 day smoothing window will not have a huge effect. We also dropped the initial S/N detection threshold for periodic signals and gave everything above 3σ a visual examination, because the S/N of a periodic signal can be difficult to calculate for a multiple-planet system with many overlapping periodic peaks. Some candidates that originally appeared at low S/N in the power spectra were actually detected at moderate S/N once we had fit for the S/N of the transit light curve with the other signals removed. We found seven companions with S/N = 3–7, and another six between S/N = 7–10. None of the low and marginal S/N candidates are listed as validated; see discussion in Section 5. In this manner, we identified 24 systems with 30 longer-period candidates, in addition to our 74 USP candidates. Thirteen of these systems are newly identified as hosting multiple candidates, and of these four are entirely new systems (both the USP and companion are new).

Both the USPs and their companions tend to be small (see Figure 1). Of the 24 candidate multiplanet systems we identified using EVEREST photometry, we documented only three cases where both the USP and the companion(s) would have been detectable using k2sff photometry: EPIC 206103150 (a.k.a. WASP-47), three transiting planets (Becker et al. 2015); EPIC 220383386 (a.k.a. HD 3167), two transiting planets (Vanderburg et al. 2016a) (as well as one nontransiting planet, Christiansen et al. 2017); and EPIC 220674823 (a.k.a. K2-106), two transiting planets (Adams et al. 2017).

4. Ground-based Observations

4.1. Spectroscopy

Accurate planetary radius values are only as good as the stellar parameters used to derive the stellar radius. To better determine the stellar parameters, we obtained reconnaissance precision spectra for some systems with the Tull Coudé spectrograph (Tull et al. 1995) at the Harlan J. Smith 2.7 m telescope at McDonald Observatory. The exposure times ranged from 100 to 4800 s, resulting in S/N from 25 to 60 per resolution element at 5650 Å. We determined stellar parameters for the host stars with the spectral fitting tool *Kea* (Endl & Cochran 2016), which compares high-resolution, low-S/N spectra of stars to a massive grid of synthetic stellar spectral models in order to determine the fundamental stellar parameters of the Kepler target stars. For typical *Kea* uncertainties and the range in $T_{\rm eff}$ over which it derives reliable stellar parameters, see Endl & Cochran (2016). We also determined absolute RVs by cross-correlating the spectra with known RV standard stars. The stellar parameters from each observation and the derived values of $T_{\rm eff}$, $\log(g)$, and [Fe/H] are shown in Table 3. When multiple observations were taken to constrain the stellar RV, we assigned the star to have the average value of the parameters for $T_{\rm eff}$, $\log(g)$, and [Fe/H] reported in Table 1 for the purpose of our analyses. A few observational targets showed significant variations in RV values over time that likely indicate stellar-mass companions, as noted in Table 1, and are not included in the 74 systems we retained as candidates.

4.2. Stellar Radius Estimation

For systems with previous analyses, we used the literature value for $R_\star$ with the smallest error bar. Otherwise, we used our observationally derived values from Table 3, where available, and then the values from the Ecliptic Plane Input Catalog, or EPIC (Huber et al. 2016), for $T_{\rm eff}$, $\log(g)$, and [Fe/H]. To calculate $R_\star$, we used the isochrones from the Dartmouth models assuming a stellar age of 5 Gyr (Dotter et al. 2008), individual stellar ages being largely unavailable. As a check, we compared the isochrones values for $R_\star$ (which are based on a numerical grid) to the values from the equation-based models of Boyajian et al. (2012). Both approaches agreed well within error, all but five with $\Delta R_\star < 0.2 R_\odot$, and all within $< 3\sigma$. We did not use the isochrones values in one case, EPIC 201214691, where isochrones produced $R_\star = 38 \pm 14 R_\odot$, which, although technically within 3σ, is an extremely inflated radius for otherwise unremarkable stellar parameters, with $T_{\rm eff} = 5122 \pm 82$ K, Fe/H $= -0.049 \pm 0.25$, and $\log(g) = 4.5 \pm 0.04$. For this system, we used the value $R_\star = 0.78 \pm 0.05 R_\odot$ from Boyajian et al. (2012) instead. All stellar radius sources are noted in Table 1.

4.3. High-resolution Imaging Constraints

High-resolution images are a critical component of planetary validation efforts (e.g., Adams et al. 2012, 2013; Dressing et al. 2014). In particular, the contrast curves produced by imaging dramatically decrease the physical area in which an undetected stellar binary blend could lurk, and thus increase the a priori odds that a transit signal is planetary. Contrast curves for available systems are shown in Table 4. If additional stars are detected, the observations may confirm a false positive (if, for instance, the location of the star matches an observed shift in

Table 3
McDonald Spectroscopic Observations

Target	UT	HJD	T_{exp}(s)	S/N	T_{eff}(K)	[Fe/H]	log(g)	rot(km s^{-1})	RV(km s^{-1})	Note[a]
201264302	2017 Apr 7 05:32:06.9	2457850.75592	3477.8	24	3875 ± 157	−0.90 ± 0.10	4.33 ± 0.21	9.00 ± 4.65	50.20 ± 0.80	
201264302	2017 May 18 03:27:50.2	2457891.66756	3600.0	31	3875 ± 157	−0.80 ± 0.20	4.17 ± 0.17	9.00 ± 3.84	49.70 ± 1.00	M
201595106	2017 Jan 19 12:31:35.0	2457773.0273	486.1	33	5820 ± 20	−0.01 ± 0.03	4.62 ± 0.12	3.62 ± 0.18	0.59 ± 0.25	
201606542	2016 Mar 15 07:31:09.2	2457462.81892	597.1	35	5540 ± 108	0.03 ± 0.04	4.81 ± 0.12	13.23 ± 0.53	13.11 ± 0.61	S
201650711	2017 Feb 17 05:15:59.1	2457801.73285	1412.0	48	4280 ± 153	−0.83 ± 0.07	4.25 ± 0.48	2.77 ± 0.43	4.88 ± 0.58	
201650711	2016 Mar 16 07:28:38.6	2457463.81728	1659.2	43	4340 ± 103	−0.81 ± 0.08	4.25 ± 0.42	2.31 ± 0.40	5.52 ± 0.43	
202094740	2016 Sep 10 10:39:49.1	2457641.94531	536.7	41	6250 ± 341	−0.20 ± 0.12	4.92 ± 0.08	120.00 ± 0.00	49.02 ± 1.48	S,F
202094740	2017 Feb 17 04:52:40.7	2457801.70827	225.0	36	6300 ± 129	−0.14 ± 0.08	4.06 ± 0.36	50.00 ± 0.00	−14.64 ± 6.29	S,F
203533312	2016 Mar 15 11:07:20.5	2457462.97775	2161.2	38	6620 ± 86	0.09 ± 0.05	4.19 ± 0.12	23.85 ± 0.83	18.56 ± 1.50	R
203533312	2016 Mar 16 11:33:30.0	2457463.99681	2299.6	37	6320 ± 111	−0.06 ± 0.06	4.12 ± 0.26	25.08 ± 0.834	19.98 ± 4.43	R
206024342	2017 Oct 17 03:59:20.6	2458043.68139	2059.5	38	5760 ± 60	−0.24 ± 0.03	4.62 ± 0.16	3.80 ± 0.20	52.98 ± 0.24	
206024342	2017 Nov 11 01:24:33.1	2458068.56905	1619.1	37	5688 ± 132	−0.20 ± 0.12	4.33 ± 0.17	2.90 ± 0.40	53.06 ± 0.35	
206151047	2016 Sep 10 07:16:53.3	2457641.81914	1756.7	33	5880 ± 73	−0.30 ± 0.04	4.56 ± 0.16	4.00 ± 0.23	− 16.86 ± .25	
206151047	2017 Nov 11 02:00:34.4	2458068.59742	2141.2	34	6062 ± 113	−0.20 ± 0.12	4.58 ± 0.08	3.90 ± 0.30	−17.01 ± 0.42	
206169375	2016 Sep 10 07:54:54.5	2457641.84179	1076.6	39	6180 ± 73	−0.27 ± 0.03	4.44 ± 0.06	5.38 ± 0.21	14.59 ± 0.30	
206169375	2017 Oct 15 04:05:09.3	2458041.67913	779.3	37	6100 ± 141	−0.25 ± 0.04	4.38 ± 0.16	6.20 ± 0.40	14.93 ± 0.42	
206298289	2017 Oct 17 04:43:18.3	2458043.72144	3600.0	18	3875 ± 157	−1.00 ± 0.10	4.42 ± 0.20	8.50 ± 2.90	−26.69 ± 1.26	M
206417197	2016 Sep 10 06:31:47.4	2457641.79023	2153.1	39	5240 ± 60	−0.20 ± 0.04	4.62 ± 0.07	1.77 ± 0.28	14.23 ± 0.27	
206417197	2017 Nov 11 02:48:00.2	2458068.63202	2351.5	38	5250 ± 94	−0.10 ± 0.10	4.67 ± 0.11	2.00 ± 0.20	14.09 ± 0.33	
210414957	2015 Dec 17 09:15:41.1	2457373.91896	4800.0	32	5838 ± 102	0.30 ± 0.07	4.12 ± 0.14	8.25 ± 0.28	43.76 ± 0.09	
210707130	2017 Feb 17 04:27:48.1	2457801.69147	902.6	44	4440 ± 93	−0.36 ± 0.09	4.38 ± 0.33	1.92 ± 0.38	−4.26 ± 0.56	
210707130	2015 Dec 18 03:50:12.9	2457374.67776	2189.7	47	4462 ± 84	−0.28 ± 0.10	4.17 ± 0.18	1.92 ± 0.34	−4.12 ± 0.08	
210707130	2016 Sep 10 08:27:53.7	2457641.86788	2335.0	51	4380 ± 73	−0.43 ± 0.09	4.31 ± 0.16	1.38 ± 0.27	−3.14 ± 0.30	
210754505	2015 Dec 18 06:30:20.8	2457374.79139	2586.7	36	5875 ± 103	0.04 ± 0.05	4.04 ± 0.19	8.75 ± 0.22	−1.82 ± 0.07	
210954046	2015 Dec 18 08:05:17.3	2457374.84919	1200.0	50	6188 ± 298	0.00 ± 0.16	3.00 ± 0.58	53.33 ± 3.55	18.83 ± 0.49	F
210954046	2015 Dec 17 03:25:23.3	2457373.65486	1200.0	38	6062 ± 274	0.00 ± 0.16	3.00 ± 0.58	55.00 ± 2.89	40.57 ± 1.05	F
210961508	2015 Dec 19 03:08:23.2	2457375.65275	2895.7	42	4925 ± 45	−0.06 ± 0.07	3.42 ± 0.08	2.42 ± 0.15	−58.53 ± 0.05	E
210961508	2017 Nov 11 06:33:04.3	2458068.78856	1735.3	40	5000 ± 80	0.00 ± 0.10	3.92 ± 0.20	2.30 ± 0.30	−58.67 ± 0.31	E
211152484	2015 Dec 18 07:28:11.5	2457374.82461	1407.3	44	6188 ± 67	−0.12 ± 0.06	4.12 ± 0.15	8.42 ± 0.15	−49.55 ± 0.05	
211357309	2017 Mar 21 05:04:38.0	2457833.7298	2499.8	50	4240 ± 223	−1.00 ± 0.00	4.62 ± 0.12	4.23 ± 0.39	18.09 ± 0.74	
212157262	2017 Nov 11 11:19:00.4	2458068.98210	1649.2	35	5438 ± 63	0.00 ± 0.10	4.58 ± 0.08	2.20 ± 0.20	−8.52 ± 0.23	
212432685	2017 May 18 05:59:41.1	2457891.76177	1196.5	35	6180 ± 136	−0.36 ± 0.04	4.50 ± 0.18	8.00 ± 0.00	102.50 ± 0.60	A
212470904	2018 May 24 05:00:23.0	2458262.7259	2151.5	25	4820 ± 124	0.18 ± 0.08	4.62 ± 0.22	2.85 ± 0.34	−11.71 ± 0.60	
212470904	2019 Apr 28 06:43:15.0	2458601.7998	2422.9	42	4800 ± 63	−0.16 ± 0.08	4.56 ± 0.16	1.46 ± 0.18	−11.71 ± 0.60	
213703832	2017 Jun 18 08:14:48.8	2457922.86992	3600.0	27	4750 ± 94	−0.30 ± 0.25	2.50 ± 0.40	13.00 ± 0.00	151.00 ± 0.50	G,R
214547683	2018 Jul 21 06:12:05.0	2458320.7856	3729.2	32	4860 ± 24	−0.12 ± 0.08	3.38 ± 0.12	3.31 ± 0.24	−20.53 ± 0.39	B
214984368	2016 Sep 9 03:27:21.6	2457640.66333	2945.0	29	4160 ± 60	−0.70 ± 0.05	1.12 ± 0.12	4.92 ± 0.18	81.40 ± 0.22	G
218952024	2017 Oct 15 02:31:39.1	2458041.61074	1093.0	25	4125 ± 82	−0.60 ± 0.10	1.67 ± 0.21	5.50 ± 0.20	50.4 ± 0.7	G,S
220198551	2016 Sep 8 11:07:19.7	2457639.97939	1915.9	33	5000 ± 63	0.01 ± 0.07	4.50 ± 0.18	1.46 ± 0.18	−11.25 ± 0.17	
220250254	2016 Aug 15 09:30:35.7	2457615.90196	397.4	29	5500 ± 45	0.00 ± 0.02	4.62 ± 0.07	2.00 ± 0.25	−1.15 ± 0.17	
220250254	2016 Oct 11 07:12:25.0	2457672.80795	332.9	41	5500 ± 89	−0.09 ± 0.02	4.50 ± 0.10	2.54 ± 0.22	−1.37 ± 0.25	
220256496	2016 Sep 8 10:26:01.9	2457639.95073	1937.7	38	5360 ± 51	−0.04 ± 0.03	4.69 ± 0.06	1.77 ± 0.28	−14.60 ± 0.13	
220256496	2016 Dec 16 02:16:39.3	2457738.60416	1175.9	33	5340 ± 51	−0.04 ± 0.03	4.81 ± 0.06	2.15 ± 0.25	−14.41 ± 0.22	

Table 3
(Continued)

Target	UT	HJD	T_{exp}(s)	S/N	T_{eff}(K)	[Fe/H]	log(g)	rot(km s^{-1})	RV(km s^{-1})	Note[a]
220383386	2017 Nov 11 03:56:05.8	2458068.66911	122.5	72	5438 ± 63	-0.10 ± 0.10	4.58 ± 0.15	2.00 ± 0.20	19.29 ± 0.16	
220492298	2017 Oct 15 06:00:03.1	2458041.76168	1020.0	17	5680 ± 37	0.29 ± 0.03	4.56 ± 0.12	3.40 ± 0.10	-19.38 ± 0.29	
220492298	2017 Oct 18 07:41:14.7	2458044.84403	3112.9	36	5560 ± 51	0.26 ± 0.05	4.44 ± 0.12	3.50 ± 0.20	-19.47 ± 0.26	
220674823	2016 Aug 15 09:46:55.0	2457615.91451	598.2	29	5580 ± 86	0.04 ± 0.03	4.62 ± 0.16	2.62 ± 0.18	-15.86 ± 0.13	
220674823	2016 Sep 8 09:17:37.4	2457639.90160	1618.3	59	5600 ± 55	0.01 ± 0.02	4.50 ± 0.10	2.23 ± 0.23	-16.01 ± 0.10	
220674823	2016 Oct 11 07:27:13.7	2457672.81868	408.9	39	5660 ± 60	-0.01 ± 0.02	4.62 ± 0.07	3.08 ± 0.21	-15.80 ± 0.28	

Note.
[a] A: asymmetric CCF, possible blend. E: somewhat evolved. F: false positive (large RV shifts). G: giant star. R: fast rotator. M: M dwarf has unreliable [Fe/H]. S: spectral binary with double-peaked cross-correlation function (CCF). B: identified as a binary star from imaging or phase-curve variations.

(This table is available in its entirety in machine-readable form.)

Table 4
Imaging Constraints Used in Validation

EPIC	Telescope	Wavelength	Date
201089381	GeminiS DSSI	692 (40) nm	2017 Jun 7
201089381	GeminiS DSSI	880 (50) nm	2017 Jun 7
201110617	Gemini NIRI	K	2017 Jan 28
201130233	WIYN NESSI	832 (40) nm	2017 Apr 3
201595106	WIYN NESSI	832 (40) nm	2017 Mar 18
201637175	GeminiN DSSI	692 (40) nm	2016 Jan 15
201637175	GeminiN DSSI	880 (50) nm	2016 Jan 15
201650711	SOAR HRCam	I: 879 (289) nm	2019 Mar 18
205152172	WIYN NESSI	832 (40) nm	2018 Jul 7
206024342	Keck II NIRC2	K	2015 Aug 7
206103150	Keck II NIRC2	K	2015 Aug 21
210707130	Keck II NIRC2	K	2015 Oct 28
211562654	Keck II NIRC2	K	2016 Jan 21
212157262	Keck II NIRC2	K	2016 Jan 21
212303338	WIYN NESSI	832 (40) nm	2018 Feb 1
212470904	WIYN DSSI	880 (54) nm	2016 Apr 21
212532636	WIYN DSSI	880 (54) nm	2016 Apr 21
220250254	WIYN NESSI	832 (40) nm	2016 Oct 20
220256496	WIYN NESSI	832 (40) nm	2016 Oct 21
220383386	GeminiS DSSI	880 (50) nm	2017 Jun 9
220383386	GeminiS DSSI	692 (40) nm	2017 Jun 9
220383386	WIYN NESSI	832 (40) nm	2016 Nov 11
220492298	WIYN NESSI	832 (40) nm	2016 Oct 20
220554210	Gemini NIRI	K	2016 Oct 19
220554210	Palomar PHARO-AO	K short	2016 Oct 19
220554210	WIYN NESSI	832 (40) nm	2016 Oct 21
220674823	Keck II NIRC2	K	2016 Oct 16
220687583	WIYN NESSI	832 (40) nm	2016 Nov 15
228721452	WIYN NESSI	832 (40) nm	2017 Mar 11
228732031	GeminiN NIRI	K	2017 Feb 19
228732031	WIYN NESSI	832 (40) nm	2017 Apr 5
228801451	Palomar PHARO-AO	K short	2017 Jul 4
228813918	WIYN NESSI	832 (40) nm	2017 May 12
228814754	GeminiS DSSI	692 (40) nm	2017 Jun 10
228814754	GeminiS DSSI	880 (50) nm	2017 Jun 10
228836835	GeminiS DSSI	692 (40) nm	2017 Jun 10
228836835	GeminiS DSSI	880 (50) nm	2017 Jun 10

the photocenter during transit, e.g., Batalha et al. 2010). Not all companion stars signify false positives, however; if the stars have similar magnitudes and the transit is shallow enough, the signal may still be from a planetary-sized body regardless of which star it is around. However, it is critical to know both (a) which star is the host star, because the host star radius determines the planet's radius and (b) by how much the companion star is diluting the transit. Calculating the dilution factor makes it possible to adjust the light-curve-derived parameters to provide the true planetary radius, which in turn is critical for accurate individual planetary and population analyses. We identified two systems with very close companions (within 4″–5″) in Table 5. An example contrast curve is shown for EPIC 201650711, which also has a close companion, in Figure 2.

We identified 28 systems for which imaging data are available using the ExoFOP website. (In a few well-studied cases, multiple contrast curves in similar wavelengths are available but not every curve was used, because additional curves were not needed to securely validate the planet.) Data came from six telescopes: WIYN, Keck, Gemini South, Gemini North, Palomar, and SOAR. Within these 28 systems, there are 46 planetary candidates (both USPs and companions), and we

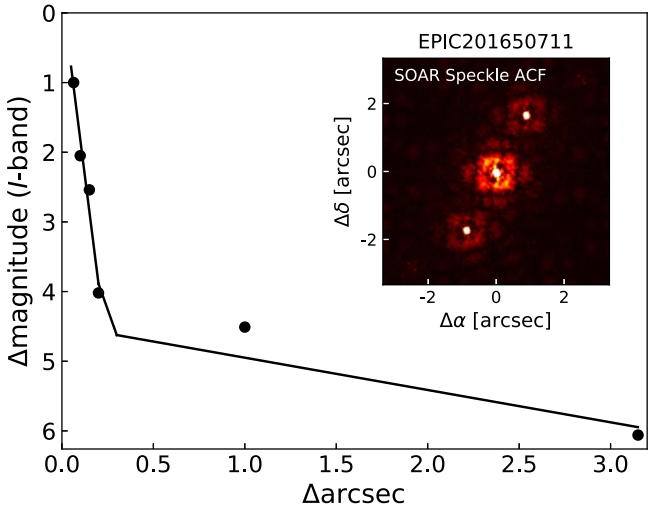

Figure 2. The 5σ detection sensitivity to nearby companions for the SOAR speckle observation of EPIC 201650711 as a function of separation from the target star and magnitude difference with respect to the target. Inset is the speckle autocorrelation function from the observation. A nearby star at 1.″79 separation is mirrored in the image. To determine the star's true quadrant, a shift-and-add routine is performed resulting in a position angle of 333°.

Table 5
Close Companions Detected through Imaging

EPIC	Distance (″)	Wavelength	ΔM	Source
201650711	1.79	I	1.2	SOAR
212303338	0.113	880nm	1.99	WIYN
212303338	0.098	692nm	2.45	WIYN

have newly validated 6, while 27 were previously validated or confirmed, leaving 13 candidates in need of either validation or confirmation.

4.3.1. WIYN and Gemini Speckle Imaging

We observed targets using two similar speckle imaging instruments at three different telescopes. The Differential Speckle Survey Instrument (DSSI; Horch et al. 2009) was deployed as a visiting instrument at the WIYN 3.5 m, Gemini North 8 m, and Gemini South 8 m telescopes. The NN-EXPLORE Exoplanet Stellar Speckle Imager (NESSI; Scott et al. 2018) was installed at WIYN in late 2016 to replace DSSI at that facility. Both DSSI and NESSI operate by splitting the incoming light into blue and red channels and recording simultaneous images of each target with an Andor iXon Ultra 888 EMCCD camera on each channel. For speckle imaging, we acquire a data set consisting of a small number (1–10) of 1000-frame data cubes on each target. The number of 1000-frame sets taken normally depends on target brightness and observing conditions. Each frame is 40 ms long at WIYN and 60 ms at the Gemini telescopes, exposure times intended to maximize S/N for the typical seeing at each site. Along with data sets taken of science targets, we observed nearby single stars to serve as point-source calibrators. For each data set, the fields of view are confined to 256×256 pixel subarray readouts of the full EMCCDs. These narrow fields are sufficient to cover the typically $\sim 2''$ wide isoplanatic atmospheric patch centered on the target with a plate scale that critically samples the diffraction-limited resolution at each telescope. At Gemini,

the field of view is $2.8 \times 2.''8$ with a plate scale of $0.''011$ pixel^{-1} and at WIYN it is $4.6 \times 4.''6$ with a plate scale of $0.''018$ pixel^{-1}. Filters with bandpass widths of 40–54 nm are used in each channel. For these data, filters with central wavelengths at 692, 832, and 880 were used.

A standardized data reduction pipeline was applied to all of these speckle data. The basic reduction and production of high-level data products were previously detailed by Howell et al. (2011). The high-level data pipeline products consist of a reconstructed, diffraction-limited resolution image of the target and surrounding field in each filter, relative photometry and astrometry of any companion sources detected near the target, and a contrast curve that gives the detection limit for point sources as a function of angular separation from the target.

4.3.2. SOAR Speckle Imaging

We searched for stellar companions to EPIC 201650711 with speckle imaging using the HRCam instrument on the 4.1 m Southern Astrophysical Research (SOAR) telescope (Tokovinin 2018) on 2019 March 18 UT. Observations were in Cousins *I* band, a similar visible bandpass to Kepler. The 5σ detection sensitivity and speckle autocorrelation functions from the observation are shown in Figure 2. A 1.2 mag fainter companion was detected in the SOAR observation at a separation of $1.''79$. This companion also appears in the Gaia DR2 catalog (GAIA DR2 source id 3812335125094701056, $g' = 13.79$, $\Delta g' = 1.35$) and has a comparable parallax and proper motion to the target star, indicating the two are likely associated; see Section 6.4.2 for further discussion of this system.

4.3.3. Keck and Palomar Imaging with Near-infrared Adaptive Optics

For high-resolution imaging in the near-infrared, we utilized two adaptive optics systems: the first was on the Hale 5 m telescope and the second was on the Keck II 10 m telescope.

The Palomar Observatory observations were made of EPIC 220554210 and EPIC 228801451 with the PHARO instrument (Hayward et al. 2001) behind the natural guide star AO system P3K (Dekany et al. 2013) in 2016 and 2017 (see Table 4). The observations were taken in a standard five-point quincunx dither pattern with steps of $5''$ in the narrowband $K_{\rm short}$ filter ($\lambda_o = 2.145$). Each dither position was observed three times, offset in position from each other by $0.''5$ for a total of 15 frames, with an integration time of 30 s per frame for EPIC 220554210 and 3 s per frame for EPIC 228801451. PHARO has a pixel scale of $0.''025$ per pixel for a total field of view of $\sim 25''$.

The Keck Observatory observations of five USP candidates (Table 4) were made with the NIRC2 instrument on Keck II behind the natural guide star AO system (Wizinowich et al. 2000) in 2015 and 2016. The observations were made in the standard three-point dither pattern that is used with NIRC2 to avoid the left lower quadrant of the detector, which is typically noisier than the other three quadrants. The dither pattern step size was $3''$ and was repeated twice, with each dither offset from the previous dither by $0.''5$. NIRC2 was used in the narrow-angle mode with a full field of view of $\sim 10''$ and a pixel scale of $0.''0099442$ per pixel. The Keck observations were made in the *K* filter ($\lambda_o = 2.196$; $\Delta\lambda = 0.336$ μm).

The AO data were processed and analyzed with a custom set of IDL tools. The science frames were flat-fielded and sky-subtracted. The flat fields were generated from a median average of dark-subtracted flats taken on-sky. The flats were normalized such that the median value of the flats is unity. The sky frames were generated from the median average of the dithered science frames; each science image was then sky-subtracted and flat-fielded. The reduced science frames were combined into a single combined image using an intrapixel interpolation that conserves flux, shifts the individual dithered frames by the appropriate fractional pixels, and median-coadds the frames. The final resolution of the combined dithers was determined from the FWHM of the point-spread function with typical final resolutions of $0.''1$ and $0.''05$ for the Palomar and Keck observations, respectively.

To within the limits of the AO observations, no stellar companions were detected. The sensitivities of the final combined AO image were determined by injecting simulated sources azimuthally around the primary target every 20° at separations of integer multiples of the central source's FWHM (Furlan et al. 2017; M. B. Lund et al. 2021). The brightness of each injected source was scaled until standard aperture photometry detected it with 5σ significance. The resulting brightness of the injected sources relative to the primary target set the contrast limits at that injection location. The final 5σ limit at each separation was determined from the average of all of the determined limits at that separation, and the uncertainty on the limit was set by the rms dispersion of the azimuthal slices at a given radial distance.

5. Validation

To validate a candidate as a planet, we used the vespa software package (Morton 2012) to compare the relative likelihood that a transiting signal is caused by a planet versus a false positive (typically some kind of eclipsing binary star blend). Validation employs many kinds of observational constraints, including the photometric light curve for each candidate, the broadband photometric magnitudes of the star, the depth of a potential secondary transit (which must be consistent with a planetary occultation), spectroscopically derived stellar parameters ($T_{\rm eff}$, [Fe/H], log(g), and, where available, image contrast curves constraining the magnitude and distance of nearby but undetected stars that could contribute to a false positive (see Section 4.3). The vespa code provides an overall FPP for each candidate. For candidates with multiple candidates detected in the same system, a multicandidate boost has been applied for targets with sufficient S/N. The threshold for applying this boost is conservatively defined, following Burke et al. (2019), to be S/N > 13 for candidates with fewer than 10 transits and S/N > 11.9 for candidates with 10 or more transits. The boosted FPP is noted separately from the individual FPP in Table 2.

Statistical validation may not be reliable for objects detected with low to moderate S/N and/or few transits (Mullally et al. 2018; Burke et al. 2019). While USPs have abundant transit numbers even in a single K2 campaign, the same is not always true of their longer-period companions; 13 companions in our sample have fewer than 10 transits available. Another more nuanced issue with validation was noted by Burke et al. (2019) and relates to the systematic false-alarm rate (SFA), the rate at which spurious signals may be identified as transit-like by a given detection pipeline. Assumptions in the validation framework about the low SFA rate, which were developed using analyses of the Kepler main mission pipeline, may not directly translate to K2 data. In particular, in this survey the detection

threshold has been pushed to lower limits (S/N = 7) to identify more of the rare USP candidates. Performing a full SFA analysis falls outside the scope of the current work; it also is not possible to directly apply the approach of Burke et al. (2019) to the single-pointing campaigns of K2, e.g., permuting the order of multiple Kepler quarters. We did however perform a sanity check on our SFA rate using an inversion test of a single campaign, Campaign 2 (chosen for having average noise and number of transiting candidates). With inversion, the flux values are flipped around the nominal baseline level, so that valleys appear as peaks and vice versa, to create realistic noise without real signals. Of 13,394 stars in Campaign 2, 1735 were identified in the inverted data by our pipeline as having periodic signals with $P < 1$ day and S/N > 7; most were immediately rejected for failing our initial depth and duration cuts, leaving 110 for visual inspection. Of those 110, almost all were easily rejected as non-planetary by the shape of the signal (most are sinusoids). Just two were passed along for further inspection and diagnostic tests, which they both failed (the pattern and amplitude of the out-of-transit variability did not match a planetary transit). Neither would have been identified as a candidate and sent to our pipeline for fitting and further tests. We conclude that our SFA rate is low enough that we may ignore it for the purposes of statistically validating planetary candidates. However, we have adopted a conservative stance toward candidates near the margins of validation and at low to moderate S/N, following the recommendations of Burke et al. (2019).

Planetary validation proceeds as follows. For each candidate, we calculate an FPP using vespa. If multiple candidates are detected in a system, each candidate with sufficient S/N (S/N > 13 if $N < 10$ transits and S/N > 11.9 otherwise) provides a statistical boost to the FPPs of other candidates in the system, decreasing the FPP by a factor of 10 (if the system contains two qualifying planets) or 15 (three or more planets). A planet is declared validated if it has FPP $\leqslant 1\%$, or a likely false positive if FPP $\geqslant 90\%$, following e.g., Montet et al. (2015). Out of an abundance of caution, we do not declare candidates to be validated if they have S/N < 10 even if their FPP is low, following Burke et al. (2019); this affects six candidates with low S/N (between 3 and 7): EPIC 206024342 p4, EPIC 201609593 p2, EPIC 201085153 p2, EPIC 220554210 p3, EPIC 220256496 p2, and EPIC 201650711 p2. We also have left as candidates three USPs with high FPPs but low S/N: EPIC 214189767, EPIC 219752140, and EPIC 228739208.

We validated 36 of 104 candidate planets, including 10 planets that had not been validated before. This number includes seven newly validated USPs (EPIC 201427007 p1, EPIC 201595106 p1, EPIC 206024342 p1, EPIC 206042996 p1, EPIC 212624936 p1, EPIC 220492298 p1, and EPIC 228836835 p1) and three companions (EPIC 206024342 p2, EPIC 206024342 p3, and EPIC 212624936 p2). Meanwhile, we found 17 candidates, all USPs, with better-than-even odds of being a false positive (FPP > 50%), of which 5 have FPP > 90%. Most of the likely false positives lack any imaging or spectroscopic constraints, which are recommended where possible before finally ruling the candidates out, because ruling out the presence of nearby background stars can dramatically change a candidate's FPP.

6. Discussion of Individual Candidates

We will now discuss the characteristics and dispositions of select individual candidates and classes of planets.

6.1. All Validated Planets are Small

We start with a few important categories where we did not find promising candidates: UHJs and planets in the short-period desert (R_p between 3 and 10 $R_\oplus$). Our 74 USP candidates are almost uniformly small, and we did not validate any candidate with $R_p > 2.4\,R_\oplus$.

6.1.1. A Single, Faint Ultra-hot-Jupiter Candidate

EPIC 210605073, from Campaign 4, was previously reported as a candidate by Adams et al. (2016). There are no spectroscopically derived stellar parameter values for $T_{\rm eff}$, [Fe/H], and log(g) because it is too faint for follow-up observations (Kep = 17.887). This system is our largest candidate and the only UHJ. For its size, its period is short enough ($P = 0.567$ days) that its confirmation would be highly significant because tidal effects are quite strong on giant planets at this distance; the shortest-period confirmed UHJ, NGTS-10 b, has $P = 0.767$ days (Figure 1). For the sake of completeness, we attempted to validate the system despite the highly uncertain stellar parameters. We inferred a value of $T_{\rm eff} = 7918$ K from the available stellar photometric magnitudes ($g = 17.859$, $r = 17.896$, $i = 18.004$, $z = 18.125$) and the corresponding temperatures in Table 1 from Pinsonneault et al. (2012); the number we use is the median of the three estimates for $T_{\rm eff}$ using the differences in each band, using 500 K for the error bar. We arbitrarily assigned [Fe/H] = 0.0 ± 0.5, and log(g) = 4.0 ± 0.5. Even with these favorable guesses, vespa returned a high FPP of 0.6, and this object remains an uncertain, though unlikely, candidate.

6.1.2. Few Plausible Short-period Desert Candidates

We do not find any compelling short-period desert candidates in this work. Just three candidates are within 1σ of the lower radius edge of the desert ($R_p > 3\,R_\oplus$): EPIC 201085153, EPIC 201089381, and EPIC 203533312.

EPIC 201085153 ($R_p = 2.4 \pm 1\,R_\oplus$, $P = 0.26$ days, Kep = 17.3) is a candidate planet in a two-candidate system (see also Section 6.3.1), but its planetary radius is low enough and its radius error high enough that it likely falls below the lower edge of the short-period desert.

The only other plausible short-period desert candidates are EPIC 201089381 ($R_p = 2.8 \pm 0.5\,R_\oplus$, $P = 0.16$ days, Kep = 14.3) and EPIC 203533312 ($R_p = 3.5 \pm 0.3\,R_\oplus$, $P = 0.176$ days, Kep = 12.2), which are also the two shortest-period planets in our sample. These two candidates are so close to their stars that the validation software fails to converge, with vespa returning a "Roche Lobe" error, indicating that its orbital solutions are all necessarily unstable. Given that the location of the Roche limit depends very strongly on the stellar and planetary parameters, a closer examination of these systems is required to determine if these are legitimate planets that we have caught on the brink of disruption (Jackson et al. 2016), or (more likely) a pair of false positives.

6.2. Shortest-period Planet that We Validated

We successfully revalidated K2-137 b, a.k.a. EPIC 228813918, at $P = 0.1797$ days, or 4.3 hr (Smith et al. 2018), with a low FPP = 0.001. Despite its proximity to its star, it did not raise any "Roche Lobe" errors from vespa as in Section 6.1.2. This planet is the second-shortest period of any confirmed planet around a main-sequence star, after KOI 1843.03 at 4.2 hr (Rappaport et al. 2013).

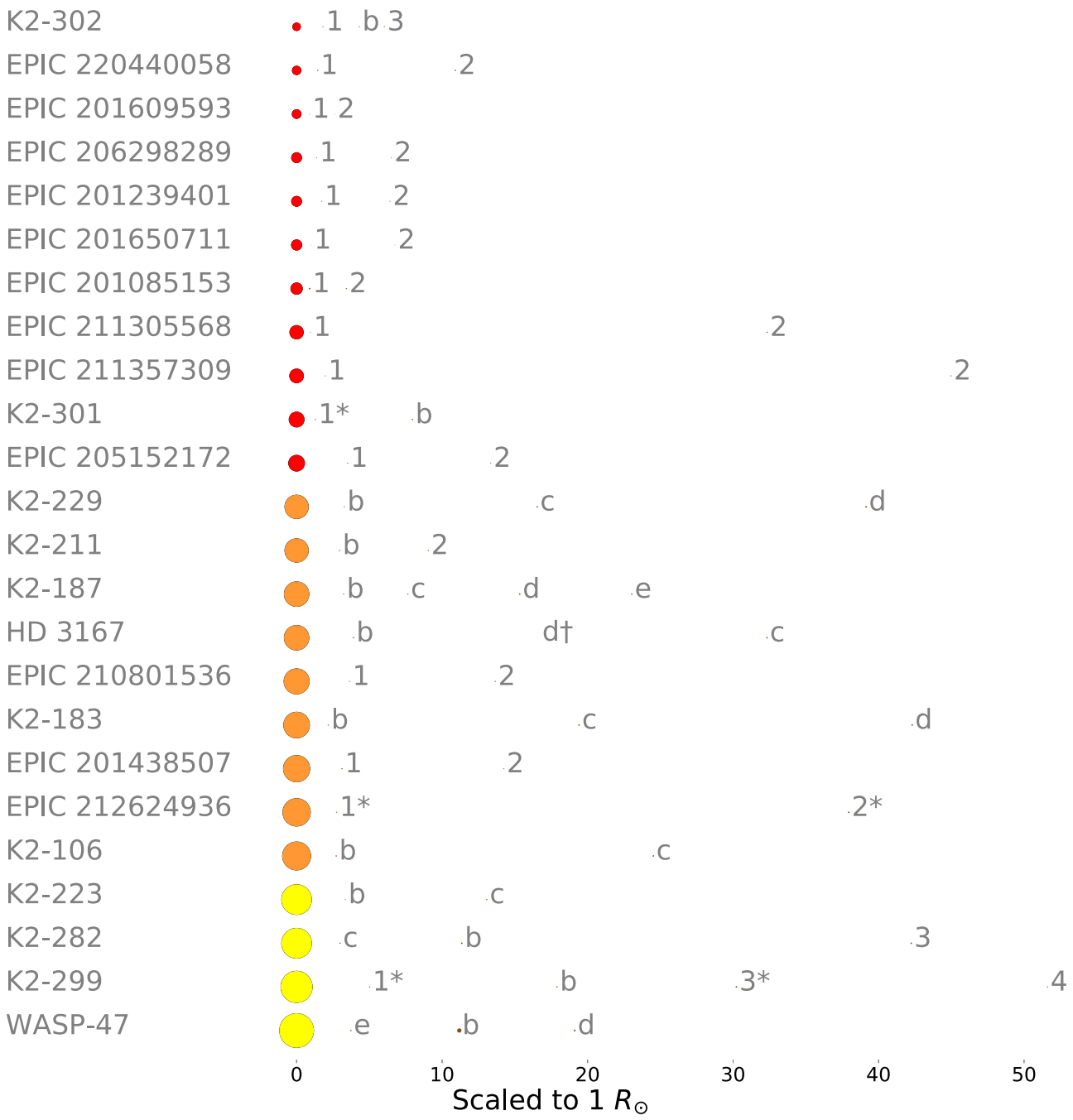

Figure 3. All known USP multiplanet systems for Campaigns 0–8 and 10, plotted entirely to scale. All sizes and distances are in solar radii ($R_\odot$). Stars are color coded by spectral type using stellar radius as a proxy: red = M ($R_\star \leqslant 0.7\,R_\odot$), orange = K ($0.7 < R_\star \leqslant 0.96\,R_\odot$), and yellow = G ($0.96 < R_\star \leqslant 1.15\,R_\odot$). No USPs were found around F stars. Numbers denote candidates and letters denote confirmed or validated worlds. Planets with an asterisk (*) have been newly validated in this work but are pending an official letter designation. One nontransiting planet is marked with a dagger (†) and plotted with zero radius at the correct separation from the star.

6.3. Twice as Many Known Multiplanet Systems

A plot of all 24 multiplanet systems in K2 Campaign C0–8 and 10, which are known to host at least one USP, is shown in Figure 3. The extremely small semimajor axes for these systems make it possible to plot the stars and planets with the physical sizes and separations shown entirely to scale.

We find that our sample of USPs commonly have neighbors, with 24 out of 74 (32%) candidates in this paper having additional transiting companions. We have found transiting companions with periods from 1.4 to 31 days, with a median of 4.5 days; two systems are also known to have RV companions, with the most distant one at 588 days (see Figure 4). In half of the multicandidate systems (13) either the USP or the companion is new, and 4 represent entirely new candidate multiplanet systems.

With the new discoveries, the estimated occurrence rate of multiplanet systems for our K2 sample is comparable to the rate of all Kepler planets (with $R_p = 0.5$–$10\,R_\oplus$) at somewhat longer periods ($P = 3$–300 days) (24% have 2+ planets; He et al. 2021); a nearly identical observed rate was found by Zink et al. (2019), who placed the expected number of planets at $\langle N_p \rangle = 5.86$ planets per star ($P < 500$ days). For the shorter

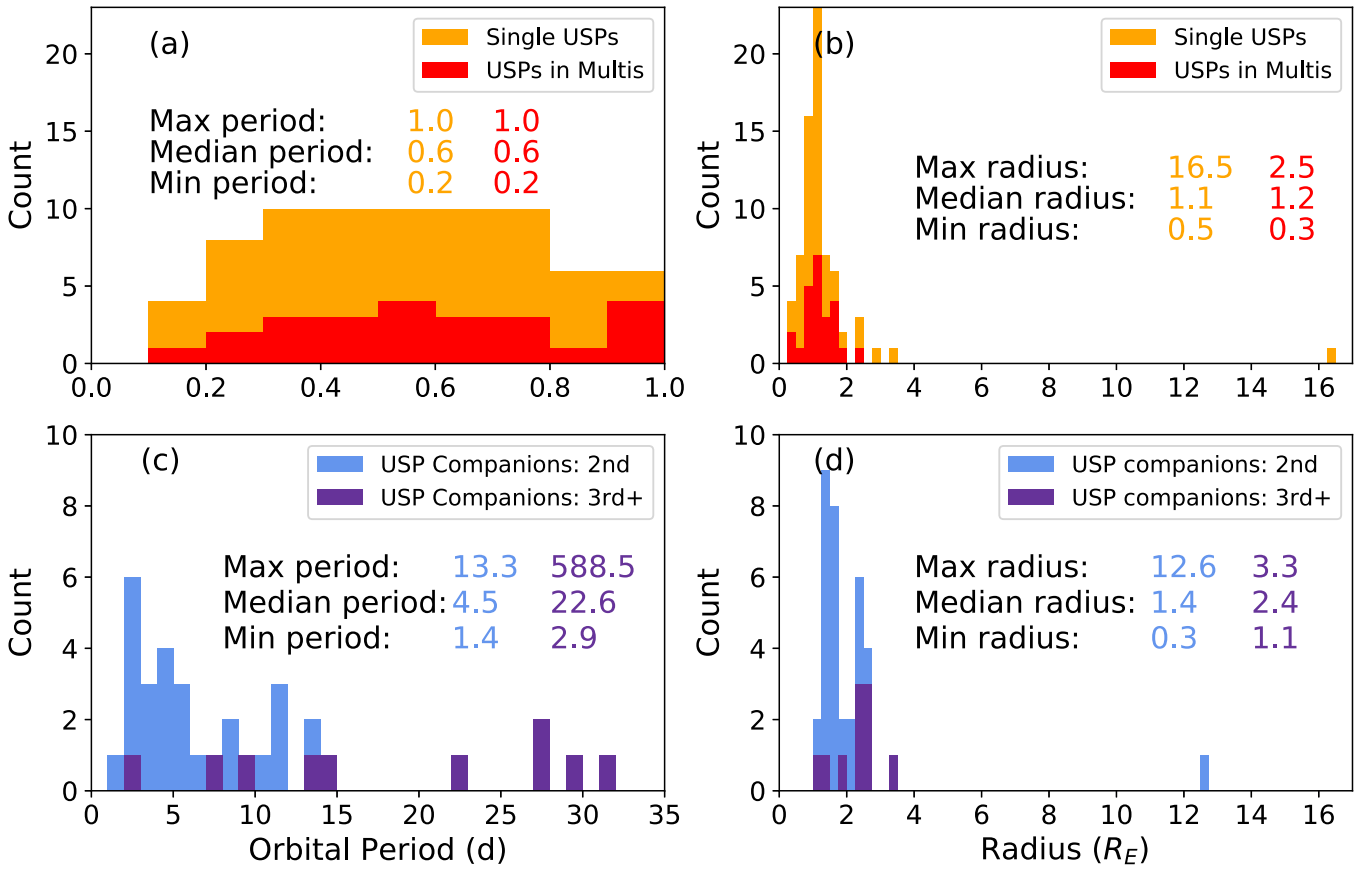

Figure 4. Stacked histograms of properties of our population of 74 USPs and their 23 known companions. (a) Distribution of orbital periods for apparently single USPs (orange) and those in multiplanet systems (red). (b) Distribution of planetary radius for apparently single USPs (orange) and those in multiplanet systems (red). (c) Distribution of orbital periods for companion planets second closest known planet (blue) and any additional companions (purple). Two companions that do not transit but have known periods from radial velocity, HD 3167 d and WASP-47 c, are included in the period statistics (though WASP-47 c is off the plot at 588 days); the most distant transiting companion is K2-229 d, at 31 days (Santerne et al. 2018). (d) Distribution of planetary radius for companion planets to USPs, showing both the second closest known planet (blue) and any additional companions (purple). Nontransiting companions have no known radius values and are not plotted.

periods ($P < 50$ days) that are more directly comparable to the USPs and companions in our survey, they found the expected number of planets per star to be 1.34 (Zink et al. 2019), in close agreement with prior work by Youdin (2011, $\langle N_p \rangle = 1.36$). The number of planets per star in our survey is 1.41. Thus, at first glance, the multiplicity of USPs is consistent with that of more distant planetary systems.

6.3.1. Four Entirely New Multiplanet Systems

EPIC 201609593, from Campaign 1, has two new candidates ($P = 0.318$ days and $P = 1.39$ days). Both were detected with marginal S/N = 9 and 4, respectively. The USP is among the smallest candidates in our sample ($R_p = 0.5\,R_\oplus$) and has one of the shortest periods ($P = 7.6$ hr), while the companion is the shortest-period companion to a USP candidate yet found. (No system has yet been found with two USPs.) Neither planet was validated due to their low S/N.

EPIC 220440058, from Campaign 8, has two new candidates ($P = 0.627$ days and $P = 3.836$ days). The USP was robustly detected with S/N = 17, while the companion has S/N = 7. No contrast curves are available, and both remain unvalidated as we do not apply a multiplicity boost due to the companion's marginal S/N.

EPIC 201085153, from Campaign 10, has two new candidates ($P = 0.257$ days and $P = 2.26$ days). The USP was detected with high S/N = 26, though the companion only has S/N = 4. We note that further follow-up of this system is difficult s it is a faint (Kep = 17.3, $J = 15.8$) M dwarf ($T_{\rm eff} = 3945 \pm 386$ K).

EPIC 201438507, from Campaign 10, has two new candidates ($P = 0.327$ days and $P = 2.536$ days). Although the USP was detected with S/N = 13, the companion has a very low S/N = 3.4. The USP has not been validated; no contrast curves are available, though the star is sufficiently bright for future observations (Kep = 14.067).

6.3.2. New USP and Known Longer-period Candidate Newly Validated

EPIC 212624936 (2 planets), from Campaign 6: Kruse et al. (2019) reported a long-period candidate at $P = 11.81$ days and S/N = 10, and we found a new USP candidate at $P = 0.57$ days and S/N = 12.9. Both planets have been validated for the first time in this work.

6.3.3. Seven New Companions to Previously Reported USP Candidates

EPIC 201239401, from Campaign 1: the USP was reported by Vanderburg et al. (2016b) and has S/N = 24, and we have newly identified a companion at $P = 6.784$ days (low S/N = 6). Due to the low S/N of the companion, we have not applied a multiplicity boost, and both remain candidates.

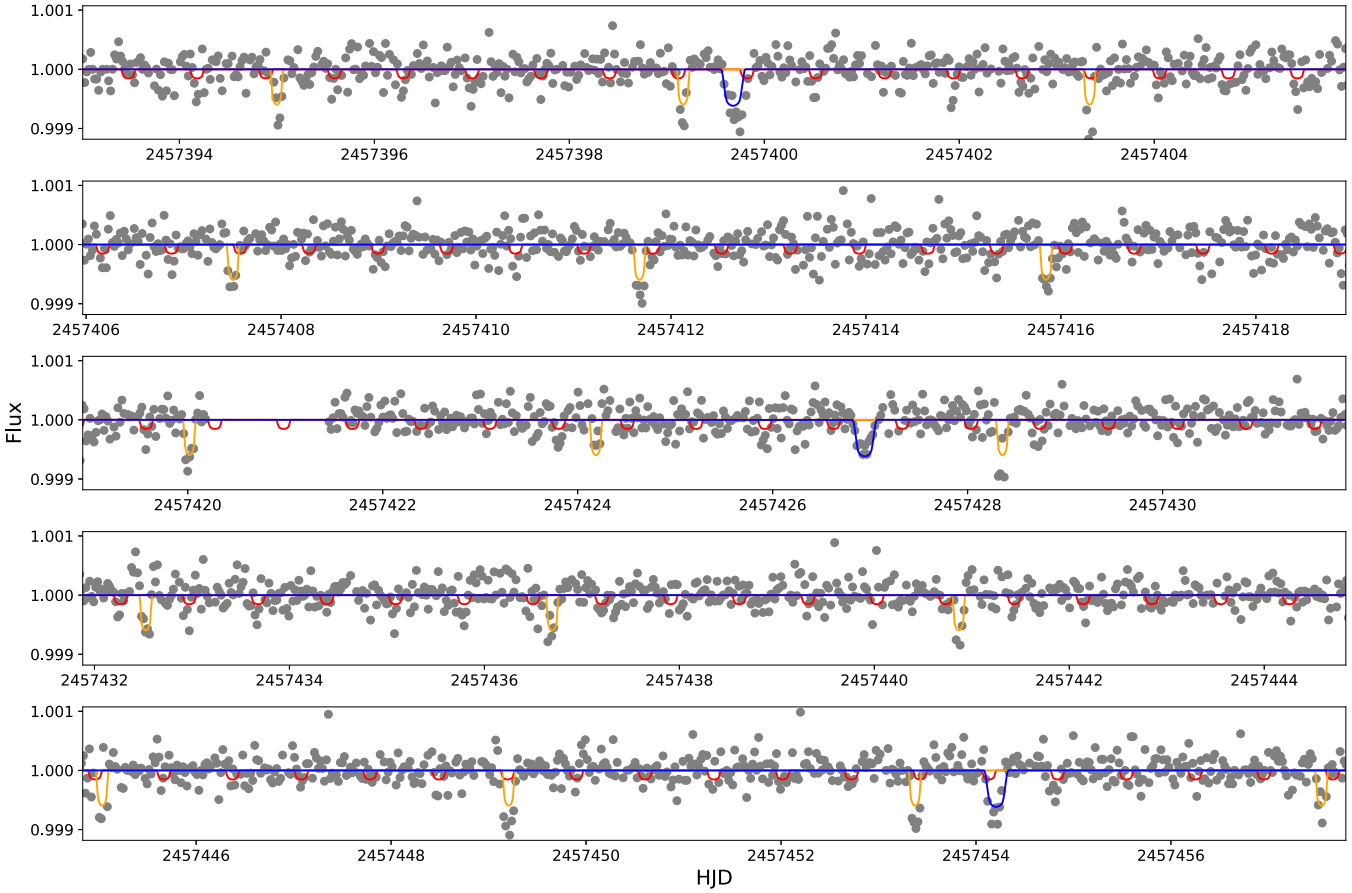

Figure 5. K2-282, a.k.a. EPIC 220554210, with three known planets. The USP is planet b (red) and is too small to be detected in individual transits, unlike c (orange) and d (blue).

EPIC 205152172, from Campaign 2: the USP (Vanderburg et al. 2016b), with S/N = 28, has a newly identified companion at $P = 3.225$ days (S/N = 10). Both the USP and the companion have been validated after applying a multiplicity boost.

EPIC 206215704/K2-302, from Campaign 3: A USP with $P = 0.623$ days was first reported by Vanderburg et al. (2016b), while two candidate outer planets, but not the USP, were reported by Kruse et al. (2019). We have confirmed the validation of the planet at $P = 2.25$ days, assigned the planetary designation K2-302 b by Heller et al. (2019). However, we do not find the signal at 3.1 days, which is spurious and likely an alias ($3.1 = 5 \times 0.62$ days, the USP period); instead, we find a different third planetary signal at $P = 2.9$ days. The planets have S/N = 14, 13, and 12, ordered by distance from the star. We have verified that three separate transit signals are present in the data and fit each candidate separately. Even after applying a multiplicity boost, the USP and outermost companions narrowly missed validation, with FPP = 0.017 and 0.011, respectively.

EPIC 206298289, from Campaign 3: the USP at $P = 0.43$ days (Vanderburg et al. 2016b) has a newly identified companion at $P = 3.215$ days, with S/N = 26 and 7.8, respectively. Due to the marginal S/N of the companion, we have not applied a multiplicity boost, and both remain candidates.

EPIC 210801536, from Campaign 4, has two candidates ($P = 0.893$ days and $P = 2.536$ days), with the USP previously reported by Kruse et al. (2019). Both candidates were detected at marginal S/N = 9.6 and 4.4, respectively. There are no contrast curves available to provide constraints on background stars. The host star appeared to be a moderately evolved G or K star, with MAST values of log $g = 3.83 \pm 0.76$ and $R_\star = 2.0 \pm 1.7\,R_{\rm Sun}$; however, the isochrones value for the stellar radius is $0.85^{+0.28}_{-0.09}$, which we have used. Follow-up observations to improve the stellar parameters and search for nearby background stars are recommended, as the host star has magnitudes Kep = 13.176 and $J = 11.7$.

EPIC 220256496/K2-221, from Campaign 8, has two candidates. The USP ($P = 0.66$ days) was reported by Mayo et al. (2018), and we have found a new candidate with $P = 2.601$ days. We validate the USP at S/N = 21, but the companion has low S/N = 8.7, and hence remains a candidate.

EPIC 220554210/K2-282, from Campaign 8, has three planets. Kruse et al. (2019) reported two planets, at $P = 4.17$ and $P = 0.705$ days (Kruse et al. 2019), and Heller et al. (2019) confirmed the USP as K2-282 b. We did not identify the USP in our search because the dominant signal is from the planet at $P = 4.17$ days. The larger planet did show up in our longer-period search out to $P = 3$ days, at an alias at $P = 2.08$ days or half its true period, but it was evidently not a USP, and this system was set aside as outside our survey parameters. After finding this system during a review of the literature, we easily recovered the two known planets and discovered a third signal at $P = 27$ days, which has three transits during 78 days of data. A plot of the transits of each of these three systems is shown in Figure 5. The planets have S/N = 21, 18, and 8.6 respectively. All three planets were validated independently, even without a multiplicity boost.

6.3.4. Three Newly Validated Planets and an Additional, Low-S/N Candidate for K2-299

EPIC 206024342/K2-299: Three candidates have been previously reported in this system ($P = 0.91$ days, $P = 4.507$ days, and $P = 14.637$ days; Vanderburg et al. 2016a; Kruse et al. 2019). The second planet ($P = 4.5$ days) was previously validated as K2-299 b by Kruse et al. (2019); we have validated the other two for the first time. By distance from the Sun, the candidates have S/N = 11.2, 11.8, and 15. We have also identified a fourth transit-like signal at $P = 27.7$ days, albeit with low S/N = 3.6. Although the fourth candidate received a low FPP from vespa, it remains a candidate due to its low S/N and long period, with only three transits detected.

6.3.5. Two Systems with Companion Candidates Observed in Campaigns 5 and 18

Although the scope of this paper is confined to K2 Campaigns 0–8 and 10, two candidate planets were found in systems from Campaign 5 that were also observed in Campaign 18. We conditioned and searched the Campaign 18 data for just those two systems in the same manner as the rest of our data, recovering the known USP candidates at high S/N. In both cases, previous tentative detection of longer-period candidates was made more secure by the addition of the extra campaign of data. (Coincidentally, the companions both have periods near $P = 11.6$ days, though the transit midtimes do not line up.)

EPIC 211357309, from Campaign 5 and 18, has a known USP candidate at $P = 0.46$ days with S/N = 26 (Adams et al. 2016; Dressing et al. 2017). We also identified a new candidate, at $P = 11.61$ days. We combined data from Campaigns 5 and 18 to search for the best period for both candidates and found that the outer companion was detected during nine transits across both campaigns, at S/N = 8.8 (Figure 6). Neither candidate is validated because the S/N of the exterior candidate precludes a multiplanet boost.

EPIC 211305568, also from Campaign 5 and 18, has two candidates identified by Dressing et al. (2017), who calculated high FPPs for both candidates. Our FPPs are similarly high, and due to the low S/N (4.6) of the outer companion, we did not apply a multiplanet boost to the USP (at S/N = 15). There is a nearby faint stellar companion (4.″8, $\Delta J = 2$, from 2MASS via ExoFOP website), which we have not corrected for because its dilution factor in visible wavelengths is unknown. The transits of the outer planet are shown in Figure 7.

6.3.6. USP We Originally Missed in a System with a Deeper Transit of an Exterior Planet

EPIC 228721452/K2-223 is a multiplanet system ($P_b = 0.505$ days and $P_c = 4.56$ days) identified by Mayo et al. (2018) and Livingston et al. (2018). In our initial survey out to longer periods ($P < 3$ days), we clearly identified a signal at $P = 2.28$ days (an alias of half the true period of K2-223 c) with S/N = 15. However, we did not identify the USP (S/N = 10) until after reviewing the literature. We easily identified both planets and found fitted parameters are almost identical to those of Mayo et al. (2018) and Livingston et al. (2018). We have validated both planets.

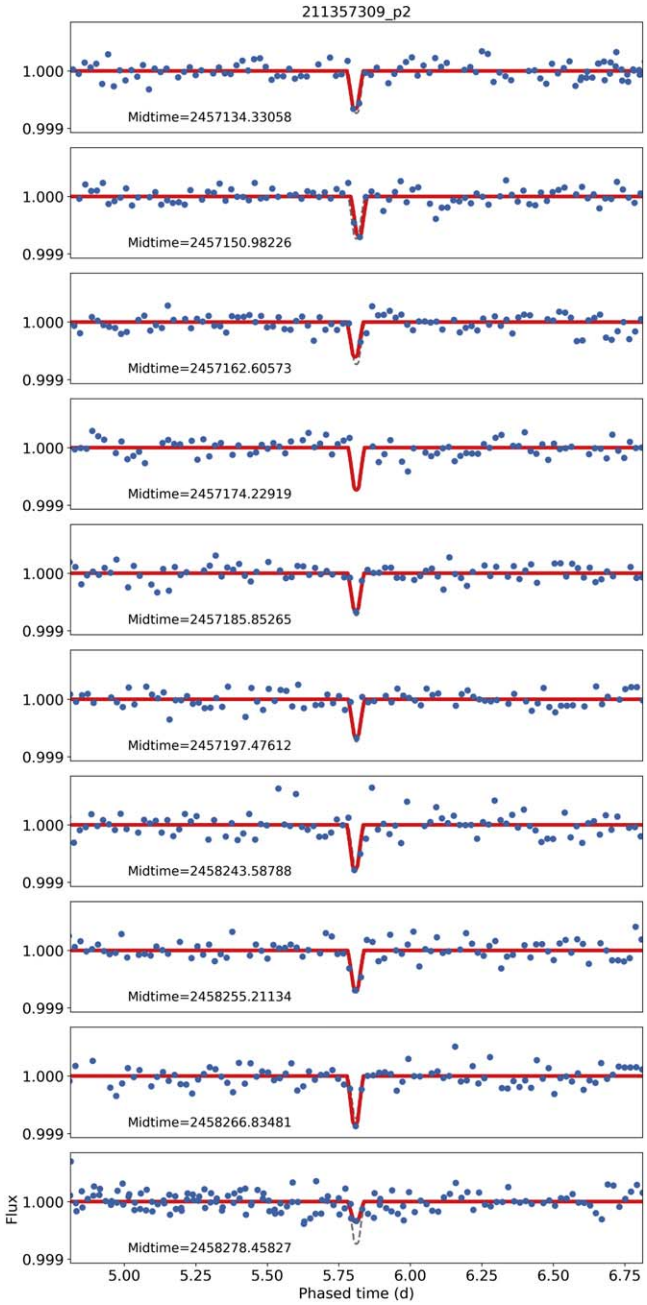

Figure 6. Candidate second planet around EPIC 211357309, with $P = 11.61$ days, combining data from Campaign 5 and 18. The best fits to each individual transit are shown in red, while the common fit to all transits is a gray dashed line.

6.4. Problematic Cases

6.4.1. Validated and Confirmed Candidates that we do not Find and/or Revalidate

EPIC 228801451, a.k.a. K2-229, from Campaign 10, has three candidates at $P = 0.58$ days, $P = 8.33$ days, and a single transit with $P = 31 \pm 1$ days (Livingston et al. 2018; Santerne et al. 2018). Although we easily identified and validated the USP, neither of the longer-period planets appears in our data. Our light curve of the USP also contains points that appear, in unbinned plots, to be artificially close to zero, due to some unknown processing problem in the smoothing step. Both of these issues are likely due to the star being active and variable;

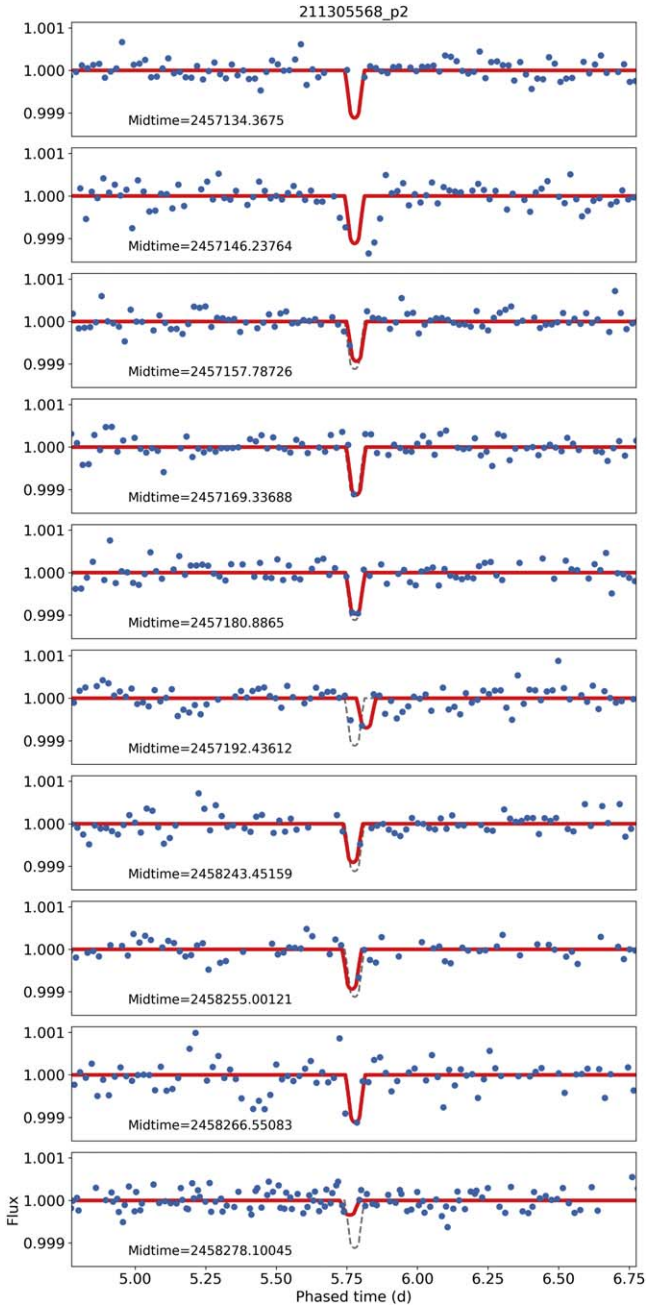

Figure 7. Candidate second planet around EPIC 211305568, with $P = 11.55$ days, combining data from Campaign 5 and 18. The best fits to each individual transit are shown in red, while the common fit to all transits is a gray dashed line.

the K2-229 system required special processing to confirm in Santerne et al. (2018).

EPIC 220250254, a.k.a. K2-210, from Campaign 8, was validated as K2-210 b (Mayo et al. 2018) with FPP $= 2.31 \times 10^{-4}$; our FPP was high enough (FPP $= 0.036$) that it remains a candidate, with a background eclipsing binary (BEB) the next most likely hypothesis. It is not clear where the discrepancy lies, and a higher-contrast image than the WIYN curve in Table 4 or other follow-up is recommended.

6.4.2. Two Candidates with Uncertain Stellar Host Parameters

EPIC 201650711, from Campaign 1: We originally flagged EPIC 201650711 p1 as a false positive in a single-planet system with an FPP of 0.92. However, during the course of this work we reexamined the system after a second planet candidate was reported by Kruse et al. (2019) at $P = 5.54$ days (which did not note the presence of a USP candidate). We call the USP candidate "p1" and the longer-period candidate "p2" to avoid confusion, because both have been referred to as candidate 1 in the literature (Adams et al. 2016; Vanderburg et al. 2016b; Kruse et al. 2019). We have verified that both sets of transits are present in the data (with S/N = 18 and 9.4, respectively). As noted in Section 4.3.2, there is a close, likely bound GAIA companion star 1.″79 away. No significant odd–even differences were detected in the transit depths for either p1 or p2 (odd–even $\sigma = 0.01$ and 0.06 respectively); no additional stellar companions were found with high-resolution imaging by SOAR (Figure 2).

Unfortunately, we have not been able to determine which star hosts the candidates (or indeed if they are in the same system); an analysis of the centroid positions of the stars using the Python package lightkurve did not turn up any significant shifts during transit, not unexpected given the close proximity of the stars (less than half a Kepler pixel). The properties of the fainter star are largely unknown apart from having the same GAIA DR2 proper motion (R.A. $= 80.1 \pm 0.3$ mas yr^{-1}, decl. $= -29.1 \pm 0.3$ mas yr^{-1}) and parallax (10.8 ± 0.2 mas) as the brighter star (all values within 1–2σ), indicating a likely bound companion.

For either host star scenario, we estimated the effect of light-curve dilution due to the other star on the calculated planetary radii. For transits around the brighter star (s1), the radius must be increased by ~15%, to $R_{p1,\ s1} = 0.36 R_\oplus$ and $R_{p2,s1} = 0.45 R_\oplus$. If the transits are around the fainter star (s2) instead, assuming the stellar properties are identical, both planets would be larger by a factor of 2, or $R_{p1,s2} = 0.64 R_\oplus$ and $R_{p2,s2} = 0.85 R_\oplus$. The radius values scale directly with the stellar radius value, so adjusting from the nominal radius of EPIC 201650711 ($R_\star = 0.34 \pm 0.05 R_{\rm Sun}$, Dressing et al. 2019) for any reasonable main-sequence stellar radius would still yield planetary-sized values.

More work needs to be done to determine which star(s) host the planets and what the stellar properties are. The relative orbital periods of the two planets, at $P = 0.26$ days and $P = 5.54$ days, are qualitatively consistent with most other observed USPs in multiplanet systems, as is the USP being the smaller planet (Section 8.2.4). Assuming that the transit is around the central star, we reran the validation analysis including the SOAR contrast curve, which was not available when we first attempted to validate. The contrast curve halved the FPP for the USP (though it remains unvalidated), though the companion remains unvalidated due to its marginal S/N. We note that the planetary radius values in Table 2 have not been adjusted for dilution.

EPIC 212303338, from Campaign 6, has a USP candidate with $P = 0.595$ days (Mayo et al. 2018) at S/N = 9. It also has a very close stellar companion (0.″1) in high-resolution images taken with WIYN in 2016, with Δmag $= 2.45$ at 692 nm (g') and Δmag $= 1.99$ at 880 nm (r') (Matson et al. 2018). We first consider how much dilution the companion star introduces to the light curve. The candidate planet is small enough ($R_p = 0.46\ R_\oplus$) and the stellar magnitudes similar enough that most scenarios are plausibly planetary. We consider two scenarios: (1) The candidate orbits the brighter star. In this case, the true radius should be increased from the value reported in Table 2 by 5%–7%, to 0.5 $R_\oplus$. (2) The candidate orbits the fainter star. In this case, the radius

should increase by a factor of about 3, to 1.5 $R_\oplus$, if we were to assume that the fainter star had the same radius as the bright star. The radius of the fainter star is also unknown; but if it is on the main sequence ($R_\star \approx 0.2$–$2\,R_\odot$), the estimated radius will change by an additional factor of 0.25–2.5, using the brighter star radius of $0.8R_\odot$; even in the maximal case, that would be $R_p \leqslant 4R_\oplus$. We note that EPIC 212303338 p1 has a relatively high validation FPP (0.67), dominated by BEB scenarios. We leave the final disposition of this candidate as undetermined. We also do not attempt to correct for dilution in the radius value reported in Table 2 due to the uncertainty of which star the signal is around.

6.4.3. EVEREST Photometry Issue for K2-131

EPIC 228732031, a.k.a. K2-131, from Campaign 10, has a confirmed USP at $P = 0.37$ days (Dai et al. 2017; Livingston et al. 2018; Mayo et al. 2018). We were unable to validate this planet using the EVEREST light curve, and closer inspection revealed high-frequency noise that appeared as quasi-sinusoidal oscillations, likely negatively affecting vespa's score. Noting that our EVEREST best-fit period was 7.8 s longer than the published period (though only by 1.6σ), we redid our analysis using the exact orbital period of Mayo et al. (2018), which reduced, although did not entirely eliminate, the high-frequency noise and also improved, but did not validate, the validation score (EVEREST FPP = 0.45). When we instead used the k2sff light curve, in which no oscillations are visible, we easily revalidated the system with FPP $= 2.6 * 10^{-4}$, demonstrating that the issue is with the photometry and not our validation framework. For consistency, the parameters for fits to the light curves derived from EVEREST photometry are the ones reported in the table Table 2.

This was the only instance we noted in EVEREST photometry of such high-frequency noise, though it is possible that other candidates with similar noise were rejected. Understanding the source of the noise would help understand whether this is a significant issue for completeness, but we leave that for future work.

6.4.4. High FPPs

Validation with vespa produced 17 USPs that are more likely than not to be false positives, with FPPs between 50% and 100%. Listed in decreasing order of FPP, the suspect USP candidates (above 90%) are in the following systems: EPIC 228739208*, EPIC 205002291*, EPIC 214539781*, EPIC 219752140, EPIC 214189767; and from 50% to 90%: EPIC 201461352, EPIC 212303338, EPIC 211336288*, EPIC 201231940*, EPIC 201609593, EPIC 210605073, EPIC 210931967*, EPIC 201469738, EPIC 211305568, EPIC 212443973, EPIC 206151047, and EPIC 201239401*. Three of these candidates (EPIC 201239401, 201609593, and 211305568) have additional candidates in their system but do not receive a multiplanet boost due to the low S/N of either the USP or the candidate. An additional three candidates in multicandidate systems had individual FPPs > 50%, but which fell below 5% after applying a multiplicity boost: EPIC 211305568 p2, EPIC 201239401 p2*, and EPIC 220440058 p2*.

Objects labeled with an asterisk (*) are candidates whose signals were only identified in our search of the EVEREST pipeline and not the k2sff pipeline, which may indicate that the signals are more likely to be spurious. This applies to 3 of the 5 candidates with FPP above 90% and 4 of 12 single candidates with FPP from 50% to 90%, as well as two potential companions in multiplanet systems.

One additional candidate we failed to validate was EPIC 201637175 a.k.a. K2-22 b, a disintegrating planet confirmed by RV mass measurements elsewhere (Sanchis-Ojeda et al. 2015a). We do not include this in our statistics as a true false positive, as we did not attempt to correct for the well-known light-curve variability when fitting.

High-resolution imaging data are available for just one system with an elevated FPP (EPIC 212303338, FPP = 0.74, which has a known stellar companion and is discussed in Section 6.4.2). For those targets on the elevated FPP list for which follow-up observations are possible, they are recommended because imaging contrast curves can make a huge difference in validation results, as noted previously for EPIC 201650711 where the FPP dropped in half once imaging was available. A more dramatic case was EPIC 213715787 a.k.a. K2-147 b, where we estimated the FPP both with and without the Subaru AO imaging constraints and found that including them dropped the FPP from 0.6 to 3×10^{-5}.

6.5. Comparisons to Other Surveys

Several recent surveys have discovered USPs in K2 Campaigns 0–10, usually in the context of searching for companions at all periods. Because these works used different photometry pipelines and/or search algorithms, it is worthwhile to compare our results to examine what lessons we can learn.

6.5.1. Comparison to Mayo et al. (2018)

Mayo et al. (2018) completed a similar survey of K2 Campaigns 0–10 using their k2sff pipeline (Vanderburg & Johnson 2014). That work searched for candidates at all orbital periods and found 14 of our 74 USP candidates. A combination of the improved photometric sensitivity of the EVEREST pipeline over k2sff (as discussed in Sections 2 and 7.2) and our smoothing and detection algorithms, which have been tailored to detect short periodic signals, probably accounts for why they found only one-fifth of the candidates that we did. Our candidates also skew smaller: 43% of our USP sample has $R_p < 1\ R_\oplus$ but only 17% of theirs did (3/17).

They also reported three candidates that we do not have listed as planets, all of which we have identified as false positives in Table 6: EPIC 206169375, which has a close stellar companion and large odd/even differences visible in the light curve, and EPIC 212645891 and EPIC 229039390, two eclipsing binary stars with true periods at twice that identified by Mayo et al. (2018).

6.5.2. Comparison to Livingston et al. (2018)

Livingston et al. (2018) analyzed only Campaign 10 of K2 using their own photometric pipeline and found six USP candidates: EPIC 201110617/K2-156, EPIC 201595106 (which we validate), EPIC 228721452 (two planets: $P = 0.5$ and $P = 4.5$ days), EPIC 228732031/K2-131 b, EPIC 228801451/K2-229 (two planets: $P = 0.58$ and $P = 8.3$ days), and EPIC 228836835 (which we validate). We identified five of the USP candidates and discussed the one we missed, EPIC 228721452, in Section 6.3.6. We found an additional nine candidates that were not present in Livingston et al. (2018), including EPIC 201438507 (two candidates), EPIC 228739208, EPIC 228814754, EPIC 228877886, EPIC 201427007

Table 6
Rejected Planet Candidates

EPIC	Reported P (days)	Real P (days)	Notes
201577017	0.4775252	0.955	EB
201606542	0.44437	0.8887	Spectroscopic binary (SB2, double peak)
202092559	0.6687	1.3374	EB
202094740	0.6897	1.3794	Spectroscopic binary (SB2, single peak)
202139294	0.5217136	1.0434	EB
202971774	0.2358684	0.47171	EB
203518244	0.84	2.1495	EB
203633064	0.7099504	1.4199	EB
204880394	0.2338108	0.71007	EB
205377483	0.3938505	0.78763	EB
206169375	0.36745	⋯	Close AO companion + high odd/even difference
206315178	0.3176828	0.63532	EB
210961508	0.349935	0.769	EB
211158357	0.2990737	0.5981	EB
211613886	0.9587591	1.9175	EB
211685045	0.769057	⋯	Variable star
211843564	0.4520313	0.90399	EB
211995325	0.279	⋯	Pipeline depth mismatch
212066407	0.8218241	1.6436	EB
212150006	0.89838	⋯	Pipeline depth mismatch, close AO companion (0.″5)
212270970	0.7165461	1.4331	EB
212362217	0.6962935	1.3928	EB
212432685	0.531684	1.0634	EB
212645891	0.32815384	0.65626	EB
213123443	0.546127	1.0923	EB
214984368	0.2633809	0.5268	EB
215125108	0.738067	1.4761	EB
215353525	0.9085915	1.8172	EB
215381481	0.533393	1.0668	EB
218195416	0.4951253	0.9903	EB
218952024	0.56007	1.1201	Spectroscopic binary (SB2, double peak)
219266595	0.944284	1.8886	EB
219420915	0.5150196	1.02988	EB
220198551	0.7988453	1.59758	EB
220201207	0.4378443	⋯	Variable star
220282718	0.5551606	1.1103	EB
220263105	1.44473	⋯	Variable star
220316844	0.6719977	1.34404	EB
220569187	0.6045	⋯	Pipeline depth mismatch
229039390	0.25605	0.5033	EB, close AO comp. (0.″6)

Note. EB = eclipsing binary from visual inspection of EVEREST photometry. Spectroscopic binary = binary found through follow-up spectroscopy, Section 4.1. Close AO companion = nearby star likely contaminating the system, from https://exofop.ipac.caltech.edu/. Pipeline depth mismatch = EVEREST and k2sff depths differ by >50%, indicating different blending fractions.

(This table is available in its entirety in machine-readable form.)

(which we validate), EPIC 201130233/K2-157, EPIC 228813918/K2-137, EPIC 201085153 (two candidates), and EPIC 201089381.

6.5.3. Comparison to Kruse et al. (2019)

Kruse et al. (2019) used the earlier EVEREST 1.0 photometry to announce 818 planet candidates in C0–8 at all orbital periods (their Table 7). By design, their survey made conservative cuts (10σ) on odd–even depth differences, allowing likely eclipsing binaries to pass through. By comparing our set of candidates to theirs, we can offer a real-world assessment of the reliability of results from the EVEREST 1.0 catalog, particularly at the shortest periods where EVEREST 1.0 performed worst (Kruse et al. 2019).

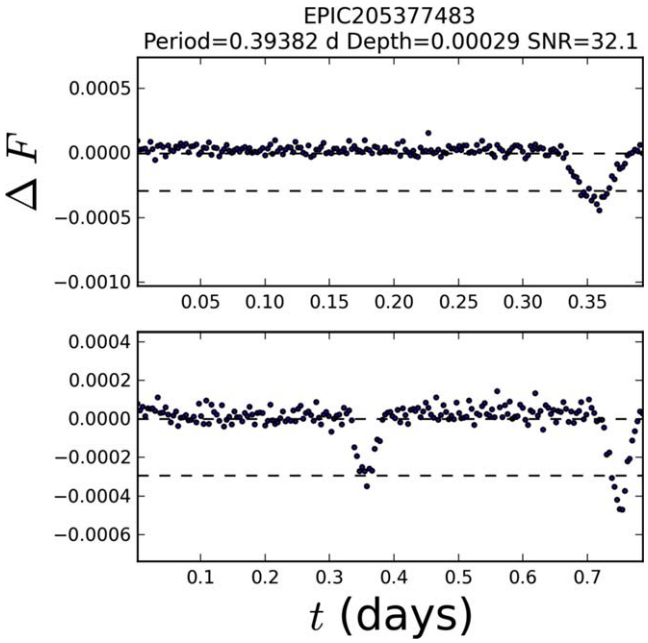

Figure 8. Diagnostic plot showing the photometry for EPIC 205377483 folded at its nominal period (top) and twice that period (bottom). A potential transiting planet (at $P = 0.39$ days) is revealed to be an eclipsing binary (at $P = 0.79$ days) with telltale differences in transit depths between alternating transits.

Removing our candidates from Campaign 10, we found 58 USP candidates in C0–8 (excluding EPIC 220554210, which we originally missed), of which Kruse et al. (2019) detected 24 (33%). Again, our sample skews smaller: 32% of our sample had $R_p < 1R_\oplus$ but only 4% of theirs did. They also reported 31 USP candidates that do not appear in our list (Table 2). We examined the folded light curves for all of these candidates and found that almost all of the signals are either due to eclipsing binary blends (28) or to stellar variability (2), often at twice the period listed in Kruse et al. (2019). These objects are included in our table of rejected candidates in Table 6. Meanwhile, none of our candidates appear in their list of false positives or eclipsing binaries (their Tables 6 and 9). Just one of their candidates that we originally missed is genuine (EPIC 220554210) as discussed in Section 6.3.3.

Because the $P < 1$ day sample of Kruse et al. (2019) had so many false positives, we briefly examined some of their longer-period candidates ($1 \leqslant P \leqslant 3$ days) to estimate what fraction might not be planets. For this paper, we did not vet any candidates with $P > 1$ day (aside from companions to USPs), but our initial search went out to $P < 3$ days. This was to guard against missing objects where the period had been aliased out of our search region, as discussed in Section 2. Our initial diagnostic plots include the light curve folded to the nominal period, P, and $2 \times P$. These plots are useful for quickly identifying eclipsing binary stars, which may exhibit different transit depths between odd and even transits, patterns of out-of-transit variability (often due to ellipsoidal variations in binary star systems), and other features that can be obscured when the data are folded to shorter periods than the true orbital period for the system. An example is shown in Figure 8, where a plausible transit of EPIC 205377483 at the originally identified period

($P = 0.39$ days) is shown to have unequal transit depths, an EB signature, when folded at twice the nominal period. By examining plots like this for the Kruse et al. (2019) sample of 69 candidates with $1 \leqslant P < 2$ days, we found 9 clear eclipsing binaries and 20 with some other kind of periodic signal, likely stellar variability—2 more candidates we identified at somewhat different periods than they did. Repeating this exercise for candidates with $2 \leqslant P \leqslant 3$ days, we found that 15 of their 68 candidates in this range were likely nonplanets (11 stellar noise/variability, 4 EBs) and 3 were candidates at different periods (including EPIC 206215704, discussed in Section 6.3.3). We thus find that the short-period planet candidates reported in Kruse et al. (2019) ($P < 3$ days) include a significant fraction of variable and eclipsing binary stars mixed among the viable planetary candidates, with the percentage of false positives decreasing with longer orbital periods (47% with $P \leqslant 1$ day, 42% with $1 \leqslant P < 2$ days, and 22% with $2 \leqslant P \leqslant 3$ days). Additional false positives are also expected after further vetting and follow-up observations, as in this work.

6.6. Rejected USP Candidates

We investigated every reported USP candidate in K2 Campaign 0–8 and 10 that we could identify in the literature. Some of these candidates (including a few that we reported in prior work, Adams et al. 2016) have turned out to be false positives, often after the advent of new spectroscopic or other observational constraints. We list the rejected candidates in Table 6. In addition to the candidates from Kruse et al. (2019) and Mayo et al. (2018) we discussed above, we note one more rejected USP candidate:

EPIC 203518244, from Campaign 2, was reported as a USP at $P = 0.84$ days using k2sff photometry by Vanderburg et al. (2016b). At $S/N = 5.8$ it was below the 10σ cutoff in Adams et al. (2016). In this work, the EVEREST photometry clearly shows the transit to be a grazing eclipsing binary at $P = 51.589$ hr or $P = 2.15$ days, an alias (5/2) of the previously reported period.

7. Survey Completeness

7.1. Detectability Calculations

To test the completeness of our survey, we injected a grid of synthetic transits into a representative sample of light curves, as in Adams et al. (2016). We sorted all light curves from a given campaign by the median noise of the detrended light curve and took 10 light curves at each decile (median noise ranging from 238 to 477 ppm), as well as the least noisy (≈1 ppm) and most noisy ($\approx 10^6$ ppm) curves for each campaign. Into each of these representative time series we inserted transits with radius ratios from 0.0025 to 0.25 and with periods between 3.5 and 23.5 hr. For computational simplicity, we fixed $i = 90^\circ$ and the limb-darkening parameters to those of the Sun. With typically shallow depths and only one to three points in any given transit, the average USP has poorly constrained inclinations and limb-darkening parameters even after stacking tens of transits together. The significant uncertainties on light-curve shape mean estimating limb-darkening parameters would have been difficult, and so we did not. Each synthetic light curve was run through our EEBLS detection pipeline, and a transit was declared detected if it was recovered within 0.1% of the injected period and within a factor of 2 of the assumed transit depth. The completeness as a function of the period and radius is shown in Figure 9. Note that two of the three campaigns closest to the Galactic Plane, and thus with the most potential for false positives due to crowding, also have the most candidates with high FPPs; by distance from the Galactic Plane, they are Campaign 0 (no candidates), Campaign 7 (three likely FPs), and Campaign 2 (one likely FP).

7.2. Comparing EVEREST 2.0 to k2sff

To investigate the importance of the improved S/N of the EVEREST 2.0 photometry pipeline, we compared the detectability for this survey to previous work by the SuPerPiG collaboration, which used a similar detection and vetting program but with k2sff photometry. Adams et al. (2016) identified 19 candidates in C0-5; here, using EVEREST, we have identified twice as many candidates (38) in the same six campaigns (and rejected some of the prior discoveries as false positives). Many of the newly identified planet candidates in C0-5 are small: in Adams et al. (2016) there were three sub-Earth-sized candidates in k2sff data (EPIC 201264302, 201650711, and 211357309), compared to 19 sub-Earth-sized USPs here; there were 7 k2sff candidates between 1 and 2 $R_\oplus$, compared to 15 here.

Detectability is a strong function of the radius ratio. In Adams et al. (2016) using k2sff data, only 10% of light curves in C0–2 would have been sensitive to a 1 $R_\oplus$ planet around a G-star (radius ratio of ∼0.01), and in C3-C5 it was 30%–65%. In this work using EVEREST data, those numbers are universally higher and much less variable by campaign, ranging from 56% (C0) to 71% (C3, C5). The improved detectability fractions agree with our discovery of many additional Earths and sub-Earths, particularly in earlier campaigns (especially C1) that had low sensitivity using k2sff photometry. The fraction of light curves unsuitable for discovering even the largest USPs is also lower: we estimated that 15%–20% of k2sff light curves were unsuitable to detect transits of any size, whereas with EVEREST that value is about 10% across all campaigns.

8. Putting the New Systems in Context

8.1. Partial Reporting of Multiplanet Systems is Common

Examining results across multiple papers has turned up a common theme: additional candidates in systems hosting USPs are often missed if one or more of the planets are close to the detectability thresholds. Due to limitations on labor, surveys for new planets often do not detect additional planets in a system unless they are well above the detection limits, to the detriment of smaller companion planets. Because false-positive rates are high for ultra-short periods, we specifically designed our survey's filters and tests to find and vet planets with periods under a day, but a consequence of running a more labor-intensive vetting program is that our targeted survey perforce underdetects longer-period planets—and this is a real problem if the dominant planet signal in a system is at a period greater than one day. At the same time, general searches for planets at all periods tend to perform worse at detecting the shortest-period planets than our dedicated search, as discussed in detail in Section 6.5. We identified several cases where multiple works have reported planetary candidates for the same system at different periods. Sometimes one or more of these reported

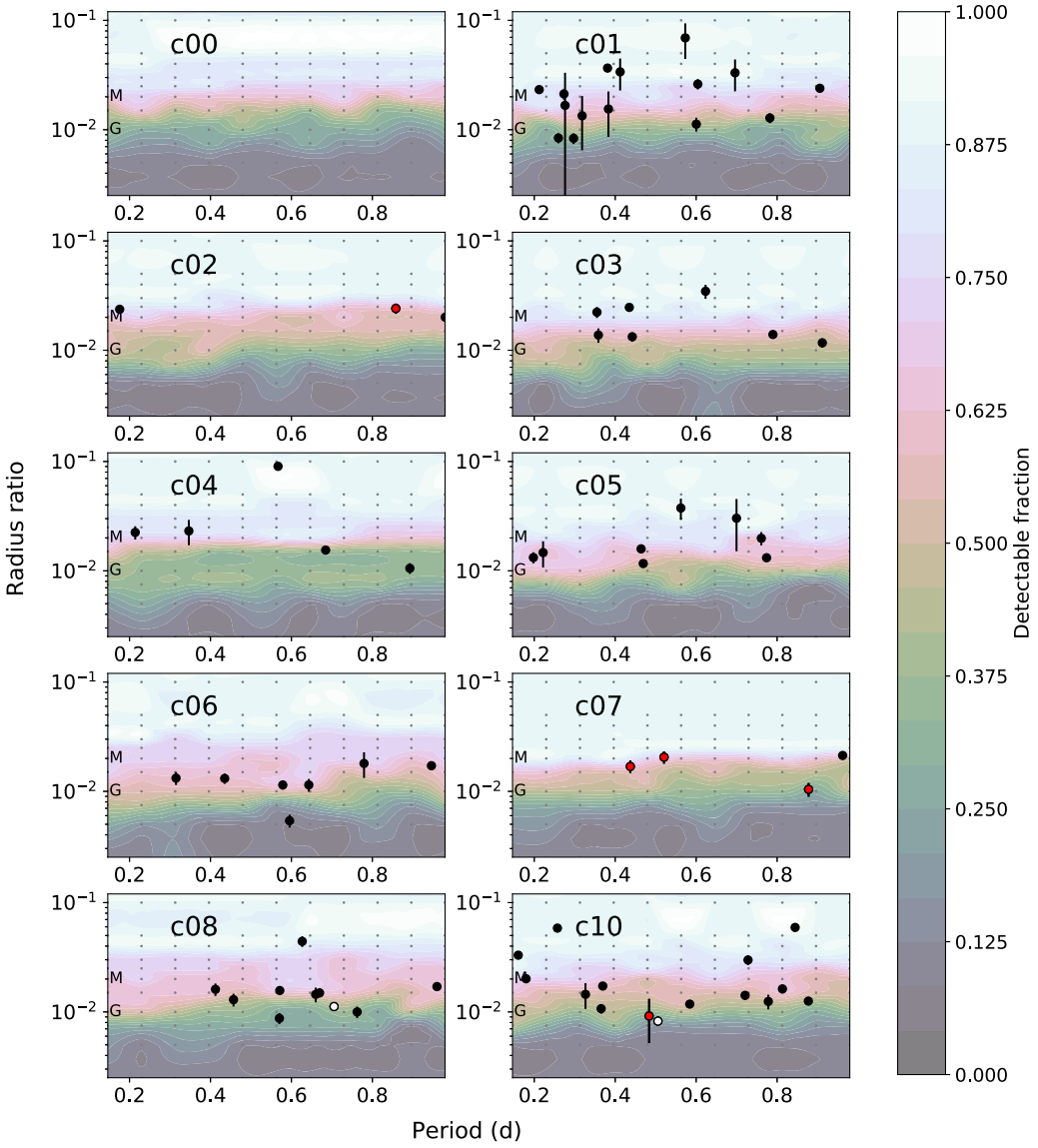

Figure 9. Detectability of injected transits by radius ratio and orbital period. Ten light curves at each noise level (the highest, lowest, and each intervening decile) were tested for a suite of injected planets with periods from 3.5 to 23.5 hr and radius ratios of 0.0025 to 0.25. The grid sampled is shown as small black dots, with the contours showing the detectability interpolated from that grid. The color bar is the same for all panels and shades from black (0% detection) to white (100% detection), depending on the fraction of samples detected. For size reference, the letters M and G on the left of each plot denote the radius ratio of a 1 $R_\oplus$ planet around a typical M and G dwarf. We plot our candidates as large black circles with error bars; candidates with high false positives (FPP $\geqslant$ 90%) are shown in red, and white circles mark the two candidates we initially missed in our survey (EPIC 220554210 in C8 and EPIC 228721452 in C10; see discussion in Section 8.1).

candidates is in error (e.g., an aliased period), and sometimes they represent a multiplanet system that was found in pieces.

8.2. Population Parameters for USPs with Companions

Systems of tightly packed inner planets have been commonly observed in Kepler and K2 data, and it has been estimated that 30% of all stars have ~3 planets with $P < 400$ days, with most more closely packed than in our solar system (Zhu et al. 2018). Such systems have been referred to as "peas in a pod," because in addition to being closely spaced (typical separation between adjacent worlds is <20 Hill radii), the planets in a single system also tend to have similar sizes, though outer planets appear to be a bit larger than inner planets (Weiss et al. 2018, though see Section 8.2.4). USP systems are of course rarer (0.5% of G stars; Sanchis-Ojeda et al. 2014), and for the few with multiple companions that have been studied, it has been noted that while the outer planets are tightly packed and have a low mutual inclination, the USP subverts the formula by being further separated and having a higher mutual inclination compared to the rest of the system (e.g., K2-266, Becker et al. 2020).

We will now discuss the observed parameters of the 24 USP-hosting systems with 2+ known planets, among which are 6 systems with 3 known planets and 2 systems with 4 known planets. In Section 8.4, we will compare how these properties agree with the predictions of different theoretical works.

8.2.1. Semimajor Axes

We first examined the distance of USPs in multiplanet systems from their stars. We found that the planetary semimajor axis follows a trend of increasing distance from the star with stellar radius so that USPs around smaller stars are

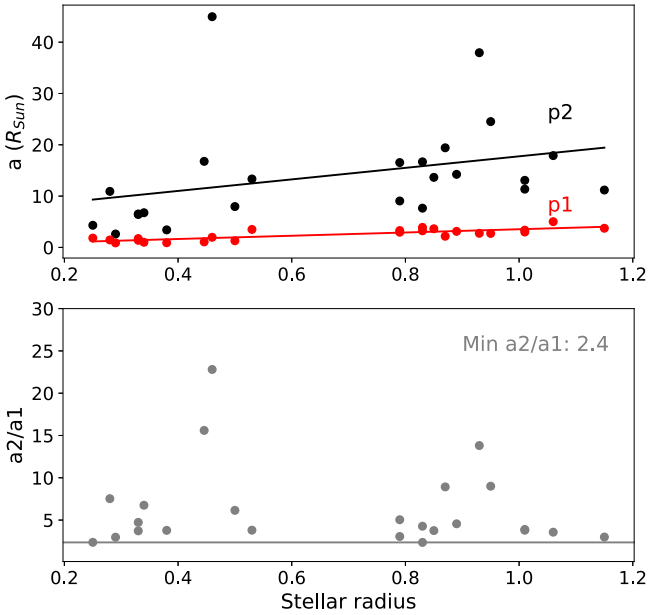

Figure 10. Comparison of stellar separations of USP and nearest companion in multiplanet systems. Top: a trend toward larger semimajor axes around larger stars is seen for both the USP (p1) and its nearest companion (p2). Bottom: the ratio between semimajor axes has a minimum value (2.4) that is constant across all stellar types.

closer to their stars. This trend holds for both the USPs and for their nearest companions, although the USPs follow a shallower trend. The ratio of semimajor axes, however, a_2/a_1, has a minimum value of 2.4 that holds across all stellar radii, as shown in Figure 10.

We next examined how closely USPs in multiplanet systems are spaced to each other. We compared our sample to the work of Weiss et al. (2018), which examined 909 planets in 355 multiplanet systems from the California Kepler Survey (CKS). We followed their formulations to estimate the planetary masses from the radius values and used that to calculate the Hill radius, which is defined following Gladman (1993) as

$$R_{\rm H} = \left(\frac{m_j + m_{j+1}}{3M_\star}\right)^{1/3} \frac{(a_j + a_{j+1})}{2}, \quad (1)$$

where planets of masses m_j and m_{j+1} orbit a star of mass $M_\star$ at semimajor axes a_j and a_{j+1}. The mutual separation between two planets, in units of mutual Hill radii, is

$$\Delta R_{\rm H} = (a_{j+1} - a_j) R_{\rm H}. \quad (2)$$

We found a similar average separation to Weiss et al. (2018), with a median $\Delta R_{\rm H} = 18$ for USP systems versus 22 for CKS sample, but a higher fraction of USP systems are more closely spaced, with 22% of the USP sample less than 10 Hill radii apart, compared to 7% in the CKS sample (Figure 11). The minimum separation found is almost identical ($\Delta R_{\rm H} = 4.5$ for USPs and $\Delta R_{\rm H} = 4.9$ for the CKS sample). We note that Chambers et al. (1996) found separations of less than 10 Hill radii to be always unstable for systems with three or more planets. We also found that the USP sample had a larger fraction of planet pairs with very large separations (>50 Hill radii): 19% of USPs versus 8% in the CKS sample; in our case these are all small, Mercury-sized planets with very low estimated masses and hence very small Hill radii. What our sample is missing, compared to the CKS sample, is planet pairs

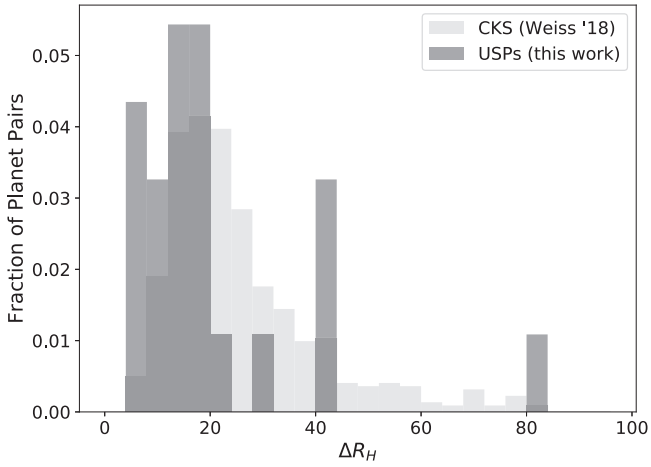

Figure 11. Separations between planets in terms of the mutual Hill radius ($\Delta R_{\rm H}$) for adjacent planets in multiplanet systems. Dark gray: 24 pairs of planets in 21 systems containing a USP from this work (three pairs with $\Delta R_{\rm H} = 254$–237 1are not shown). Light gray: 554 pairs of planets from the California Kepler Survey (CKS), Weiss et al. (2018), none of which had $\Delta R_{\rm H} > 100$.

at intermediate separations. Whether this is a selection bias effect (Kepler targets were observed for much longer than K2 targets, making longer-period detections possible) or an artifact of different formation histories is left for future research.

8.2.2. Mutual Inclinations

The inclination distribution of 24 systems with one USP and one or more transiting companions are shown in Figure 12. We find that USPs have smaller inclinations than their companions, which is consistent with their geometrical advantage because more distant companions need to be more tightly aligned to be observed to transit (see Section 8.3). We calculated the mutual inclination as the difference between the two fitted inclinations and calculated the joint error using the maximal values of the asymmetrical errors (corresponding to the lower error bar, after requiring that $i \leqslant 90^\circ$ from the fitted values). We also find that the mutual inclinations of systems with USPs are quite low (mean $\Delta i = 1\overset{\circ}{.}2 \pm 1\overset{\circ}{.}2$), with few cases significantly different from zero, and none with $\Delta i > 8^\circ$. The mutual inclinations presented here are much lower than those in the sample reported by Dai et al. (2018), which comprises a different set of objects with little overlap, as discussed in Section 8.4. It is possible that our sample is more strongly biased against objects with higher inclination dispersion, as we include many small candidates at moderate to low S/N and would not easily detect grazes, which can result in even shallower transit depths. We also note that many of our objects have higher errors than the difference in inclinations.

8.2.3. Orbital Periods and Lack of Apparent Mean-motion Resonances

The distribution of periods and radii for all 74 USPs is shown in Figure 4. There is no difference in the observed period distribution of USPs with and without companions, which is essentially flat between 0.2 and 1 day, with a median of 0.58 days. For companion planets, the median period is 4.5 days for the second planet in the system and 18.6 days for the third or fourth planet, with a maximum of 31 days for transiting

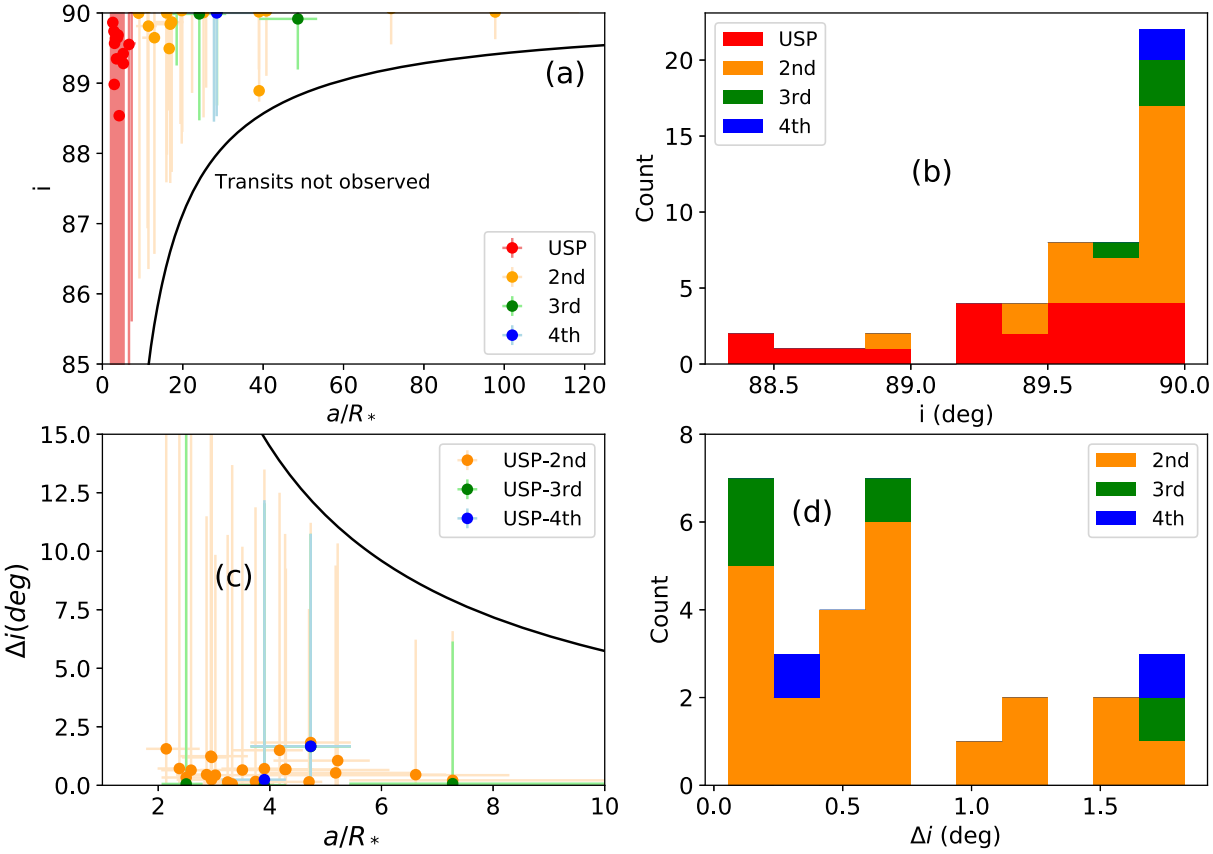

Figure 12. Inclination and semimajor axes for multiplanet systems hosting a USP. (a) i vs. a/R_* for the USP (red) and the second (orange), third (green), and fourth (blue) companions, by distance from the star. The black line shows where transits are geometrically not observable. (b) Histogram of individual inclinations. (c) Mutual inclinations $\Delta i = |i_x - i_1|$ for the USP minus the second (orange), third (green), and fourth (blue) companions. All mutual inclinations are well below the black line, where the USP would not transit even if the companion had $i = 90°$. (d) Histogram of mutual inclinations.

companions (WASP-47 c, at 588 days, is one of only two companions known that does not transit).

Little evidence is seen for current mean-motion resonances involving USPs. We examined period ratios between candidate planets in multiplanet systems. If the ratio between the periods is within ± 0.1 of an integer or half-integer ratio (i.e., 0.0 ± 0.1 or 0.5 ± 0.1), it was considered near resonance. This was intended as a first look because actual resonance or past resonance membership would need to be determined with dynamical modeling. For period ratios up to a factor of 10, just four USPs meet that criteria, which is fewer than if the period ratios were randomly distributed (40% of numbers end in those digits, which would be 0.4×30 combinations $= 12$ planets). None of the USPs are very near low-order resonances, with the closest being (1) EPIC 206024342/K2-299, where the period ratio of the USP to the second-closest planet is within 5% of a 5:1 ratio; (2) EPIC 220554210/K2-282, where the period ratio of the USP to the second closest planet is within 9% of a 6:1 ratio; (3) EPIC 201239401, where the period ratio of the USP to the second closest planet is within 1% of a 15:2 ratio; and (4) EPIC 228721452/K2-223, where the period ratio of the USP to the second closest planet is within 2% of a 9:1 ratio.

Some additional near-resonances can be found among the outer companions, though with four out of nine combinations flagged it is consistent with random chance. (4) In EPIC 212157262/K2-187, the second and third planets are within 1% of a 5:2 ratio. Two pairs are within 10% of a 2:1 ratio: (5) EPIC 211562654/K2-183, second and third planets, and (6) EPIC 212157262/K2-187, third and fourth planets. (7) EPIC 220554210/K2-282 has the second and third planets within 3% of a 13:2 ratio.

Only 6out of 24 systems have any members near a resonance, as broadly construed here. Clearly, if dynamical processes required mean-motion resonances to emplace the USPs, they have long since decoupled from the resonances in all of the systems we examined. A more detailed dynamical study would be required to determine if any of the near-resonant period ratios actually correspond to potential current or past resonances.

8.2.4. Planetary Radius

We did not confirm any UHJs ($R_p \gtrapprox 10 R_\oplus$) and found just one UHJ candidate with moderately high FPP; however, by optimizing our search to discover small planets it is possible that some of the deepest transits might have been sigma-clipped, so we do not consider our UHJ count to be complete. Medium to large planets ($R > 3R_\oplus$) also appear to be rare among planetary companions to USPs, with just one known among 24 systems (WASP-47 b). We also did not identify any compelling candidates in the short-period desert ($\sim$3–10 $R_\oplus$), as discussed in Section 6.1.2.

Excluding the lone UHJ candidate, EPIC 210605073, and focusing on the smaller population, we find a few correlations of note. First, USPs with companions are marginally more likely to be larger (median: 1.36 $R_\oplus$, sample $N = 24$) than those without (median: 1.07 $R_\oplus$, sample $N = 50$), with KS test

p-value = 0.02. This is unlikely to be a detection effect because there may, if anything, be a slight bias toward finding a smaller USP in a system with a larger known companion than to find one on its own.

Second, we do not find evidence that the intrinsic population of USPs must have smaller radius values than their companions. Although it is true that the observed median radius of all USPs ($1.14\,R_\oplus$, $N = 74$) is different from that of their known companions (second planets: median $= 1.5\,R_\oplus$, $N = 24$, p-value = 0.04; third/fourth planets: median $= 2.6\,R_\oplus$, $N = 11$, p-value $= 3 \times 10^{-4}$), this difference is entirely consistent with different detection efficiencies based on stacking shallow transits. At the median orbital period for a USP, a second planet, and a third planet (at 0.58 days, 4.5 days, and 22.6 days respectively), a K2 campaign of 80 days would yield a maximum of 138, 18, and 4 transits (ignoring gaps). Assuming that stacking yielded improvements proportional to the square root of the number of transits, the USP would be detectable at 2.8 and 5.9 times shallower depths than the second and third planets; because the radius is proportional to the square root of the depth, the detected companions would have larger radius values by a factor of 1.7 for second planets and 2.4 for third/fourth, very similar to the observed differences in median values. We do not account here for any of the other detection biases that are also at play, including inclination effects (making more distant and smaller planets less likely to transit) as well as sampling effects (making USPs with the shortest periods harder to detect, because each transit has only 1–3 points per transit with K2's 30 minute observing cadence).

8.3. Transit Detection Probabilities and a Rough Estimate of Sample Completeness

To calculate the transit probabilities, we ignore grazing transits (which would push most of these small transits into being too shallow to detect) and eccentricity (negligible for tidally locked USPs but might be important for more distant companions) and use $P_{\rm tr} = R_*/a$ (Borucki & Summers 1984). For USPs, the probability of transit is quite high: EPIC 203533312, with $a/R_* = 1.6$, has a 38% chance of transit, while even the lowest-probability USP (228814754) has a 5% transit probability. The longer-period companions in our sample have transit probabilities ranging from 0.5% to 6% (some with large uncertainties due to a/R_* being poorly constrained).

One takeaway is that the sample of USPs that we detected is much more complete than that of companions. As a first approximation (ignoring all other detection biases), we add the inverse of the transit probabilities to estimate the total number of planets and find an estimated total of 535 USPs, of which our sample of 74 would represent 14% of the total population. For the companion planets, we find that the estimated total from inverse transit probabilities is 1396, of which we only have 30 in our sample, or 2%. Considering only the second planet in each system, the detected fraction is similar (1015 estimated total second planets, of which we have found 4%). One possible conclusion is that, if our sample of USPs is seven times as complete as our sample of companions (14%/2% ~2) and companions have been found around one-third of all USPs, then every USP could be in a multiplanet system.

8.4. Comparison to Theoretical Predictions

8.4.1. Petrovich, Deibert & Wu 2019

The first paper to provide a mechanism for the origins of USPs involving high-eccentricity migration was Petrovich et al. (2019). In particular, they found that USP planets should have spin–orbit angles and inclinations relative to outer planets in the range of 10°–50°. They also predicted that most USPs should have companions that are either more distant than $P > 20$ days or with high mutual inclination ($i > 20°$). As seen in Figure 12, we see very low mutual inclinations in multicandidate systems (albeit with large error bars). We also see many companions at shorter orbital periods, although our sample is far from complete and transit detectability decreases rapidly for more distant companions.

8.4.2. Pu & Lai (2019)

Pu & Lai (2019) also presented a model that requires the presence of additional companions to emplace planets on short-period orbits. In this scenario, the future USP starts out as the innermost one in a chain of planets, with a modest orbital eccentricity (~0.1), and encounters resonances that increase the mutual inclination with respect to the exterior planets. This theory predicts that (1) planets exterior to the USP must orbit close enough that secular interactions can maintain a nonzero eccentricity for the USP for a long enough time that tidal interactions can emplace the USP; (2) the USPs should be less massive than the exterior planets; and (3) the USP may have an orbit that is significantly misaligned with the rest of the planetary system.

Our results have broad agreement with Pu & Lai (2019) on point 1, qualified agreement on 2, and qualified disagreement on point 3:

1. Planets must orbit close enough: we have found that a third of our sample of K2 USPs has a transiting companion within $P < 31$ days, and our results are consistent with most of the apparently singleton systems hosting nearby planets that do not transit (Section 8.3). The separations between planets are small both physically (Figure 10) and dynamically (Figure 11), with an average mutual Hill radius of $\Delta R_{\rm H} = 18$; nearly a quarter have $\Delta R_{\rm H} < 10$.
2. The observed sample of USPs have smaller radii than their companions, but this is consistent with detection biases toward finding small planets with more frequent transits (Section 8.2.4). A further caveat is that smaller radii may not correspond to smaller masses. Measured masses are unavailable for more than a handful of planets.
3. While we observe that USP inclinations span a larger range than those of the companions (Figure 12), it is not clear how significant this finding is, due to high errors on most of our inclinations. All of our systems are statistically consistent with zero mutual inclination, in contrast with Dai et al. (2018), one of the works that Pu & Lai (2019) drew on, who found an inclination dispersion of 6.°7 (using a sample that extends to longer periods than our own, although their USPs also have a higher range of mutual inclinations). Panel (c) of Figure 12 reproduces their Figure 3 for our sample, which has a mean $\Delta i = 1.°2 \pm 1.°2$. One possible cause for the discrepancy could be sample size and/or quality; their sample comprises few K2 candidates and has little overlap with ours. Many of our objects are shallow and/or have low

to moderate S/N, meaning that a planet in a grazing orbit (i.e., significantly different from $i = 90°$) might be more likely to be missed. We also do not account for the possibility of oppositely aligned orbits; a pair of planets at 88° and 89° will have the same Δi in Figure 12 as a pair at 92 and 89°. Because, however, most of our nominal values hew closely to 90°, this is unlikely to account for the full difference. A more in-depth analysis of the inclinations of USPs from K2 is recommended before drawing conclusions on this point.

8.4.3. Millholland & Spalding (2020)

The model of Millholland & Spalding (2020) is obliquity-driven tidal migration, where it is the planetary obliquity (the angle between the planet's orbit and its rotational spin) that drives migration of the innermost planet with at least one close companion, using the quick passage through Cassini states (configurations in which precession of the planet's spin axis matches precession of its orbital plane), which can result in substantial tidal dissipation. Five testable predictions are made by that work; we broadly agree with points (1) and (5), disagree with (3) and (4b), and leave the corroboration of points (2) and (4a) for future work.

1. USPs should have close companions ($P \lesssim 10$ days), which may or may not transit. This agrees well with Figure 4, which finds the closest companion has a median $P = 4.5$ days. About a quarter (6 of 24) of the closest companions have $10 < P_2 < 15$ days, still broadly compatible with this theory.
2. No trends are expected for eccentricity, whereas the Pu & Lai (2019) eccentricity-driven tidal migration model would expect some remnant eccentricity in the companion planets. Unfortunately, we cannot test this with our current fits because we assumed zero eccentricity for all planets to avoid fitting extra parameters to light curves that are often near the S/N limit. Some of the companion light curves are of sufficient quality that they could be examined for nonzero eccentricity.
3. USPs should have nonzero mutual inclinations. In particular, (a) they should have modest misalignments with their planetary companions, in agreement with Dai et al. (2018) but not our results in Figure 12, and (b) they should be aligned with the stellar spin (which is mostly unknown). Measuring the stellar obliquity of the USPs in multiplanet systems is an excellent goal to constrain this theory.
4. In this model, the USP rapidly breaks out of the Cassini states. This implies that (a) few USPs should be currently undergoing rapid tidal decay; long-term monitoring of the transit timing of these systems would be needed to address this question. Another prediction is that (b) planets will pile up near 1 day, with occurrence rates decreasing at shorter periods, as found in the earlier work of Sanchis-Ojeda et al. (2014). As noted in Section 8.2.3 we instead observed an even spread in the orbital period for both USPs in known multiplanet systems and USPs that are apparently single.
5. Finally, USPs are predicted to be more common around smaller host stars as in Sanchis-Ojeda et al. (2014). Although we have not debiased our discoveries to produce a detection rate by stellar type, we found that only 4 of 24 multiplanet host stars have $R_* > 1 R_\odot$.

9. Summary and Conclusions

The importance of USPs has long been recognized as potential laboratories for exploring the effects of extreme proximity to a star on planet formation and stability. However, there have to date been few large-scale population studies to determine the properties and occurrence rates of such systems. This work provides a new search of 10 campaigns of K2 data to systematically discover USPs and any companions in the same system. We present 74 candidates, 21 of which have been validated and/or confirmed as planets. Almost half (43%) of our USPs have radius values smaller than Earth, with the smallest similar to Mercury in radius. Twenty-four are in systems with at least one other transiting planet candidate, with 30 total companions detected. We note that 17 USPs have FPP > 50%, including 5 that are nominally false positives with FPP > 90% and should be treated with caution. It is important to note that 14 of our USPs and 6 of the companions are presented with S/N < 10, a deliberate decision to increase the yield of these rare-but-important objects, which will require future observations to fully clarify their status.

At this point, it should be clear that (a) USPs are commonly found in multiplanet systems (32% of the USPs in this paper have at least one known companion); (b) such systems often have 3+ planets (33% of USPs in multiplanet systems have 3 or more transiting candidates), meaning that finding one companion does not mean that you have found them all; and (c) the sample of USPs is much more complete (based solely on transit probabilities) than the sample of companions to USPs. Our results are consistent with every USP system also having at least one nearby nontransiting companion (within $P \sim 30$ days).

We recommend that all systems with known planets or candidates should be searched specifically for USP companions, which tend to be smaller and easy to miss in nontargeted searches. Furthermore, USP systems should be monitored for longer-period transits and for the RV signatures of nontransiting companions, which are expected to be common. Understanding the population of USPs is key to understanding the forces that shape planetary evolution right at the edge of stability.

Data products produced as part of this work, including the transit light curves and fitting images, are available at our repository at https://github.com/elisabethadams/superpig-public.

Thanks to Rodrigo Luger, Tim Morton, Katja Poppenhaeger, Joe Renaud, Ethan Kruse, and Dan Foreman-Mackey for helpful discussions during the preparation of this manuscript. The two anonymous reviewers also greatly improved the quality of this paper and their thorough reviews are much appreciated.

This work has made use of data from the European Space Agency (ESA) mission Gaia (http://www.cosmos.esa.int/gaia), processed by the Gaia Data Processing and Analysis Consortium (DPAC, http://www.cosmos.esa.int/web/gaia/dpac/consortium). Funding for the DPAC has been provided by national institutions, in particular the institutions participating in the Gaia Multilateral Agreement.

This research made use of lightkurve, a Python package for Kepler and TESS data analysis (Barentsen et al. 2019); Astropy, a community-developed core Python package for Astronomy (Astropy Collaboration et al. 2013, 2018); Scipy (Virtanen et al. 2020); PyMC (Salvatier et al. 2016); Batman (Kreidberg 2015); and Matplotlib (Hunter 2007).

This study is based upon work supported by NASA under grant No. NNX15AB78G issued through the Astrophysical Data Analysis Program by Science Mission Directorate and under grant No. NNX17AB94G through the Exoplanets Research Program. M.E. and W.D.C. were supported by NASA K2 Guest Observer grants NNX15AV58G, NNX16AE70G, and NNX16AE58G to The University of Texas at Austin.

This research was supported in part by the National Science Foundation under grant No. NSF PHY-1748958 under the auspices of UC Santa Barbara's Kavli Institute for Theoretical Physics.

Some of the data analyzed in this paper were collected by the K2 mission, funding for which is provided by the NASA Science Mission Directorate. The data were obtained from the Mikulski Archive for Space Telescopes (MAST). STScI is operated by the Association of Universities for Research in Astronomy, Inc., under NASA contract NAS5-26555. Support for MAST for non-HST data is provided by the NASA Office of Space Science via grant NNX09AF08G and by other grants and contracts. Some of the data presented herein were obtained at the W.M. Keck Observatory, which is operated as a scientific partnership among the California Institute of Technology, the University of California, and the National Aeronautics and Space Administration. The Observatory was made possible by the generous financial support of the W.M. Keck Foundation. The authors wish to recognize and acknowledge the very significant cultural role and reverence that the summit of Maunakea has always had within the indigenous Hawaiian community. We are most fortunate to have the opportunity to conduct observations from this mountain.

Facility: Kepler, Keck:II (NIRC2), Gemini:South, Gemini: Gillett, SOAR, Hale, WIYN.

Software: Batman 2.1.0 (Kreidberg 2015) https://lweb.cfa.harvard.edu/~lkreidberg/batman/; pymodelfit 0.1.2 (Tollerud 2011) https://pythonhosted.org/PyModelFit/core/pymodelfit.core.FunctionModel1D.html; PyMC 2.3.4 (Fonnesbeck et al. 2015) https://pymc-devs.github.io/pymc/; PyLightCurve 2.3.2 (Tsiaras et al. 2016) https://github.com/ucl-exoplanets/pylightcurve; Emcee 2.2.1 (Foreman-Mackey et al. 2013) https://emcee.readthedocs.io/en/stable/; Kea (Endl & Cochran 2016), Uncertainties 2.4.6.1 http://pythonhosted.org/uncertainties/, vespa 0.4.9 (Morton 2012) https://github.com/timothydmorton/VESPA; astropy 3.1.1 (Astropy Collaboration et al. 2013, 2018) http://www.astropy.org; scipy 1.2.1 (Virtanen et al. 2020) https://scipy.org/; matplotlib 3.0.2 (Hunter 2007) https://matplotlib.org/.

ORCID iDs

Elisabeth R. Adams https://orcid.org/0000-0002-9131-5969
Brian Jackson https://orcid.org/0000-0002-9495-9700
David R. Ciardi https://orcid.org/0000-0002-5741-3047
William D. Cochran https://orcid.org/0000-0001-9662-3496
Michael Endl https://orcid.org/0000-0002-7714-6310
Mark E. Everett https://orcid.org/0000-0002-0885-7215
Elise Furlan https://orcid.org/0000-0001-9800-6248
Steve B. Howell https://orcid.org/0000-0002-2532-2853
Rachel A. Matson https://orcid.org/0000-0001-7233-7508
Joshua Schlieder https://orcid.org/0000-0001-5347-7062
Nicholas J. Scott https://orcid.org/0000-0003-1038-9702
Carl Ziegler https://orcid.org/0000-0002-0619-7639

References

Adams, E. R., Ciardi, D. R., Dupree, A. K., et al. 2012, AJ, 144, 42
Adams, E. R., Dupree, A. K., Kulesa, C., & McCarthy, D. 2013, AJ, 146, 9
Adams, E. R., Jackson, B., & Endl, M. 2016, AJ, 152, 47
Adams, E. R., Jackson, B., Endl, M., et al. 2017, AJ, 153, 82
Adams, F. C., & Bloch, A. M. 2015, MNRAS, 446, 3676
Armstrong, D. J., Lopez, T. A., Adibekyan, V., et al. 2020, Natur, 583, 39
Astropy Collaboration, Price-Whelan, A. M., Sipőcz, B. M., et al. 2018, AJ, 156, 123
Astropy Collaboration, Robitaille, T. P., Tollerud, E. J., et al. 2013, A&A, 558, A33
Baluev, R. V., Sokov, E. N., Jones, H. R. A., et al. 2019, MNRAS, 490, 1294
Barensten, G., Hedges, C., Vinícius, Z., et al. 2019, KeplerGO/lightkurve: Lightkurve v1.1.1, Zenodo, doi:10.5281/zenodo.3371790
Batalha, N. M., Rowe, J. F., Gilliland, R. L., et al. 2010, ApJL, 713, L103
Becker, J., Batygin, K., Fabrycky, D. C., et al. 2020, AJ, 160, 254
Becker, J. C., Vanderburg, A., Adams, F. C., Rappaport, S. A., & Schwengeler, H. M. 2015, ApJL, 812, L18
Borucki, W. J., & Summers, A. L. 1984, Icar, 58, 121
Boss, A. P. 1998, AREPS, 26, 53
Boyajian, T. S., von Braun, K., van Belle, G., et al. 2012, ApJ, 757, 112
Burke, C. J., Mullally, F., Thompson, S. E., Coughlin, J. L., & Rowe, J. F. 2019, AJ, 157, 143
Chambers, J. E., Wetherill, G. W., & Boss, A. P. 1996, Icar, 119, 261
Christiansen, J. L., Vanderburg, A., Burt, J., et al. 2017, AJ, 154, 122
Claret, A., & Bloemen, S. 2011, A&A, 529, A75
Dai, F., Masuda, K., & Winn, J. N. 2018, ApJL, 864, L38
Dai, F., Winn, J. N., Gandolfi, D., et al. 2017, AJ, 154, 226
Dawson, R. I., & Fabrycky, D. C. 2010, ApJ, 722, 937
Dawson, R. I., & Johnson, J. A. 2018, ARA&A, 56, 175
Dekany, R., Roberts, J., Burruss, R., et al. 2013, ApJ, 776, 130
Demory, B.-O., Gillon, M., de Wit, J., et al. 2016a, Natur, 532, 207
Demory, B.-O., Gillon, M., Madhusudhan, N., & Queloz, D. 2016b, MNRAS, 455, 2018
Dotter, A., Chaboyer, B., Jevremović, D., et al. 2008, ApJS, 178, 89
Dressing, C. D., Adams, E. R., Dupree, A. K., Kulesa, C., & McCarthy, D. 2014, AJ, 148, 78
Dressing, C. D., Hardegree-Ullman, K., Schlieder, J. E., et al. 2019, AJ, 158, 87
Dressing, C. D., Vanderburg, A., Schlieder, J. E., et al. 2017, AJ, 154, 207
Endl, M., & Cochran, W. D. 2016, PASP, 128, 094502
Endl, M., Robertson, P., Cochran, W. D., et al. 2012, ApJ, 759, 19
Fonnesbeck, C., Patil, A., Huard, D., & Salvatier, J. 2015, PyMC: Bayesian Stochastic Modeling in Python v2.3.4, Astrophysics Source Code Library, ascl:1506.005
Foreman-Mackey, D., Hogg, D. W., Lang, D., & Goodman, J. 2013, PASP, 125, 306
Furlan, E., Ciardi, D. R., Everett, M. E., et al. 2017, AJ, 153, 71
Gladman, B. 1993, Icar, 106, 247
Hamer, J. H., & Schlaufman, K. C. 2019, AJ, 158, 190
Hayward, T. L., Brandl, B., Pirger, B., et al. 2001, PASP, 113, 105
He, M. Y., Ford, E. B., & Ragozzine, D. 2021, AJ, 161, 16
Heller, R., Hippke, M., & Rodenbeck, K. 2019, A&A, 627, A66
Hirano, T., Dai, F., Gandolfi, D., et al. 2018, AJ, 155, 127
Horch, E. P., Veillette, D. R., Baena Gallé, R., et al. 2009, AJ, 137, 5057
Howard, A. W., Sanchis-Ojeda, R., Marcy, G. W., et al. 2013, Natur, 503, 381
Howell, S. B., Everett, M. E., Sherry, W., Horch, E., & Ciardi, D. R. 2011, AJ, 142, 19
Huber, D., Bryson, S. T., Haas, M. R., et al. 2016, ApJS, 224, 2
Hunter, J. D. 2007, CSE, 9, 90
Jackson, B., Greenberg, R., & Barnes, R. 2008, ApJ, 678, 1396
Jackson, B., Jensen, E., Peacock, S., Arras, P., & Penev, K. 2016, CeMDA, 126, 227
Jackson, B., Stark, C. C., Adams, E. R., Chambers, J., & Deming, D. 2013, ApJ, 779, 165
Jenkins, J. 2019, AAS/Division for Extreme Solar Systems Abstracts, 51, 103.07
Jia, S., & Spruit, H. C. 2017, MNRAS, 465, 149

Kovács, G., Zucker, S., & Mazeh, T. 2002, A&A, 391, 369
Kreidberg, L. 2015, PASP, 127, 1161
Kruse, E., Agol, E., Luger, R., & Foreman-Mackey, D. 2019, ApJS, 244, 11
Lee, E. J., & Chiang, E. 2017, ApJ, 842, 40
Lissauer, J. J., Marcy, G. W., Rowe, J. F., et al. 2012, ApJ, 750, 112
Livingston, J. H., Endl, M., Dai, F., et al. 2018, AJ, 156, 78
Lopez, E. D., & Fortney, J. J. 2014, ApJ, 792, 1
Luger, R., Agol, E., Kruse, E., et al. 2016, AJ, 152, 100
Luger, R., Kruse, E., Foreman-Mackey, D., Agol, E., & Saunders, N. 2018, AJ, 156, 99
Mandel, K., & Agol, E. 2002, ApJL, 580, L171
Matson, R. A., Howell, S. B., Horch, E. P., & Everett, M. E. 2018, AJ, 156, 31
Mayo, A. W., Vanderburg, A., Latham, D. W., et al. 2018, AJ, 155, 136
Mazeh, T., Holczer, T., & Faigler, S. 2016, A&A, 589, A75
McCormac, J., Gillen, E., Jackman, J. A. G., et al. 2020, MNRAS, 493, 126
Millholland, S. C., & Spalding, C. 2020, ApJ, 905, 71
Montet, B. T., Morton, T. D., Foreman-Mackey, D., et al. 2015, ApJ, 809, 25
Mortier, A., Santos, N. C., Sousa, S. G., et al. 2013, A&A, 558, A106
Morton, T. D. 2012, ApJ, 761, 6
Mullally, F., Thompson, S. E., Coughlin, J. L., Burke, C. J., & Rowe, J. F. 2018, AJ, 155, 210
Neveu-VanMalle, M., Queloz, D., Anderson, D. R., et al. 2016, A&A, 586, A93
Owen, J. E. 2019, AREPS, 47, 67
Patra, K. C., Winn, J. N., Holman, M. J., et al. 2017, AJ, 154, 4
Pepe, F., Cameron, A. C., Latham, D. W., et al. 2013, Natur, 503, 377
Petrovich, C., Deibert, E., & Wu, Y. 2019, AJ, 157, 180
Pinsonneault, M. H., An, D., Molenda-Żakowicz, J., et al. 2012, ApJS, 199, 30
Pu, B., & Lai, D. 2019, MNRAS, 488, 3568
Rappaport, S., Levine, A., Chiang, E., et al. 2012, ApJ, 752, 1
Rappaport, S., Sanchis-Ojeda, R., Rogers, L. A., Levine, A., & Winn, J. N. 2013, ApJL, 773, L15
Rodriguez, J. E., Becker, J. C., Eastman, J. D., et al. 2018, AJ, 156, 245
Salvatier, J., Wiecki, T. V., & Fonnesbeck, C. 2016, PeerJ Computer Science, doi:10.7717/peerj-cs.55
Sanchis-Ojeda, R., Rappaport, S., Pallè, E., et al. 2015a, ApJ, 812, 112
Sanchis-Ojeda, R., Rappaport, S., Winn, J. N., et al. 2014, ApJ, 787, 47
Sanchis-Ojeda, R., Winn, J. N., Dai, F., et al. 2015b, ApJL, 812, L11
Santerne, A., Brugger, B., Armstrong, D. J., et al. 2018, NatAs, 2, 393
Scott, N. J., Howell, S. B., Horch, E. P., & Everett, M. E. 2018, PASP, 130, 054502
Sinukoff, E., Howard, A. W., Petigura, E. A., et al. 2017, AJ, 153, 271
Smith, A. M. S., Cabrera, J., Csizmadia, S., et al. 2018, MNRAS, 474, 5523
Tamburo, P., Mandell, A., Deming, D., & Garhart, E. 2018, AJ, 155, 221
Tokovinin, A. 2018, PASP, 130, 035002
Tollerud, E. 2011, PyModelFit: Model-fitting Framework and GUI Tool v0.1.2, Astrophysics Source Code Library, ascl:1109.010
Tsiaras, A., Waldmann, I. P., Rocchetto, M., et al. 2016, pylightcurve: Exoplanet Lightcurve Model v2.3.2, Astrophysics Source Code Library, ascl:1612.018
Tull, R. G., MacQueen, P. J., Sneden, C., & Lambert, D. L. 1995, PASP, 107, 251
Vanderburg, A., Bieryla, A., Duev, D. A., et al. 2016a, ApJL, 829, L9
Vanderburg, A., & Johnson, J. A. 2014, PASP, 126, 948
Vanderburg, A., Latham, D. W., Buchhave, L. A., et al. 2016b, ApJS, 222, 14
Virtanen, P., Gommers, R., Oliphant, T. E., et al. 2020, Nature Methods, 17, 261
Weiss, L. M., Marcy, G. W., Petigura, E. A., et al. 2018, AJ, 155, 48
Wizinowich, P., Acton, D. S., Shelton, C., et al. 2000, PASP, 112, 315
Youdin, A. N. 2011, ApJ, 742, 38
Zhu, W., Petrovich, C., Wu, Y., Dong, S., & Xie, J. 2018, ApJ, 860, 101
Zink, J. K., Christiansen, J. L., & Hansen, B. M. S. 2019, MNRAS, 483, 4479